

## Investigating sources of ozone over California using AJAX airborne measurements and models: Assessing the contribution from long-range transport

Ju-Mee Ryoo <sup>a, b,\*</sup>, Matthew S. Johnson <sup>a</sup>, Laura T. Iaci <sup>a</sup>, Emma L. Yates <sup>a, b</sup>, Warren Gore <sup>a</sup>

<sup>a</sup> Earth Science Division, NASA Ames Research Center, Moffett Field, CA, United States

<sup>b</sup> Bay Area Environment Research Institute, Moffett Field, CA, United States



### HIGHLIGHTS

- High O<sub>3</sub> at 1–4 km shows complex origins; only small influence from N. America and stratosphere.
- Transport from Asian boundary layer followed by mixing with mid tropospheric air.
- The Q diagnostic is a measure of the mixing of the air masses.
- Integrated analysis with models, reanalysis & diagnostics allows source assessment.
- WRF-STILT identifies surface impact a few days after sampling.

### ARTICLE INFO

#### Article history:

Received 10 June 2016

Received in revised form

31 January 2017

Accepted 6 February 2017

Available online 7 February 2017

#### Keywords:

Ozone

Measurements and models

Stratospheric intrusion

Long-range transport from Asia

Surface impact

### ABSTRACT

High ozone (O<sub>3</sub>) concentrations at low altitudes (1.5–4 km) were detected from airborne Alpha Jet Atmospheric eXperiment (AJAX) measurements on 30 May 2012 off the coast of California (CA). We investigate the causes of those elevated O<sub>3</sub> concentrations using airborne measurements and various models. GEOS-Chem simulation shows that the contribution from local sources is likely small. A back-trajectory model was used to determine the air mass origins and how much they contributed to the O<sub>3</sub> over CA. Low-level potential vorticity (PV) from Modern Era Retrospective analysis for Research and Applications 2 (MERRA-2) reanalysis data appears to be a result of the diabatic heating and mixing of air in the lower altitudes, rather than be a result of direct transport from stratospheric intrusion. The Q diagnostic, which is a measure of the mixing of the air masses, indicates that there is sufficient mixing along the trajectory to indicate that O<sub>3</sub> from the different origins is mixed and transported to the western U.S.

The back-trajectory model simulation demonstrates the air masses of interest came mostly from the mid troposphere (MT, 76%), but the contribution of the lower troposphere (LT, 19%) is also significant compared to those from the upper troposphere/lower stratosphere (UT/LS, 5%). Air coming from the LT appears to be mostly originating over Asia. The possible surface impact of the high O<sub>3</sub> transported aloft on the surface O<sub>3</sub> concentration through vertical and horizontal transport within a few days is substantiated by the influence maps determined from the Weather Research and Forecasting–Stochastic Time Inverted Lagrangian Transport (WRF-STILT) model and the observed increases in surface ozone mixing ratios. Contrasting this complex case with a stratospheric-dominant event emphasizes the contribution of each source to the high O<sub>3</sub> concentration in the lower altitudes over CA. Integrated analyses using models, reanalysis, and diagnostic tools, allows high ozone values detected by in-situ measurements to be attributed to multiple source processes.

© 2017 Elsevier Ltd. All rights reserved.

### 1. Introduction

Ozone (O<sub>3</sub>) is a secondary pollutant influenced by local sources as well as background hemispheric concentrations through

\* Corresponding author. Atmospheric Science Branch, NASA Ames Research Center, Moffett Field, CA, 94035, United States.

E-mail address: [ju-mee.ryoo@nasa.gov](mailto:ju-mee.ryoo@nasa.gov) (J.-M. Ryoo).

transboundary transport. Recently, the U.S. Environmental Protection Agency (EPA) has decided to lower the threshold for ground-level O<sub>3</sub> in the primary U.S. EPA National Ambient Air Quality Standards (NAAQS) from 75 ppbv to 70 ppbv to improve air quality and reduce surface O<sub>3</sub> mixing ratios (US EPA, 2015). The background O<sub>3</sub> mixing ratios in North America have been estimated to be in the range of 15–35 ppbv (Fiore et al., 2003), but recent studies report them in the range of 25–50 ppbv (Lefohn et al., 2014; Zhang et al., 2011; Emery et al., 2012), contributing more than half of the total concentration of O<sub>3</sub> referenced to the current NAAQS. Particularly in the context of existing O<sub>3</sub> concerns in the western U.S., the reduced standard emphasizes the importance of understanding the processes and sources impacting the surface O<sub>3</sub> (Fiore et al., 2002; Jaffe et al., 2003a). Furthermore, because O<sub>3</sub> can be highly affected by the local meteorology, topography, and seasonal variability (Cooper et al., 2010; Yates et al., 2013; Lin et al., 2015), a thorough understanding of western U.S. O<sub>3</sub> behavior is still lacking.

Previous literature provides that there are evidence of air aloft influencing surface O<sub>3</sub> in the western U.S. (Cooper et al., 2005; Jaffe et al., 2003a; Langford et al., 2012; Lefohn et al., 2011, 2012; Yates et al., 2014). Analyses of available observations indicate an increase of springtime O<sub>3</sub> mixing ratios in the free troposphere and at surface sites of the western U.S. since the 1980s (Jaffe et al., 2003a; Oltmans et al., 2008; Parrish et al., 2009; Fine et al., 2015). Interestingly, the increase of O<sub>3</sub> in the free troposphere over the western U.S. is coincident with rising Asian anthropogenic emissions of O<sub>3</sub> precursors as inferred from satellite measurements of column nitrogen dioxide (NO<sub>2</sub>) and bottom-up inventories (Richter et al., 2005; Ohara et al., 2007; Q. Zhang et al., 2009; Lin et al., 2015). Earlier work indicates that the contribution of Asian emissions to surface O<sub>3</sub> in the U.S. is reflected through an enhancement not only in background levels (Goldstein et al., 2004; Zhang et al., 2008; Ewing et al., 2010; Lin et al., 2012a) but also in local pollution episodes in California (Parrish et al., 2010; Huang et al., 2010; Pfister et al., 2011). Furthermore, a recent study shows that tropospheric O<sub>3</sub> concentrations over China have rapidly increased by ~7% between 2005 and 2010, due to both increase in Chinese emissions (about 21%) and increased transport of stratospheric O<sub>3</sub>. The same study also found that the tropospheric O<sub>3</sub> concentrations at two sites in China increased by 1–3% per year since 2000, contributing to positive trends in the O<sub>3</sub> levels observed at the West Coast of the U.S. (Verstraeten et al., 2015).

Meteorological processes play an important role in the transport of pollution from Asia to the western U.S. Pollution originating in the boundary layer of East Asia from direct emissions such as combustion and industrial sources is lifted to the free troposphere via processes such as deep convection or warm conveyor belts associated with midlatitude cyclones (Carmichael et al., 2003; Liu et al., 2003; Cooper et al., 2004a; Ding et al., 2009; Chen et al., 2009; Lin et al., 2010). Recently, it has been reported that Asian plumes of pollution can be transported by jet stream movement due to climate variability; when the jet stream meanders southward over the western U.S., the O<sub>3</sub> from Asia can enter into the lower troposphere, especially in the spring after La Niña winters. (Lin et al., 2015). This suggests that the transport of pollution from Asia to the western U.S. can be efficient, especially when the atmospheric conditions are favorable to the transport of air masses through large-to meso-scale circulation linked to climate variability.

Observational studies show that lofted pollutants, such as Asian dust and sulfate aerosols, come across the North Pacific Ocean in the mid- and upper troposphere, and eventually descend toward the surface of the western U.S. (Brown-Steiner and Hess, 2011), with relatively high frequency and large magnitude in some cases (Husar et al., 2001; Jaffe et al., 2003b; McKendry et al., 2008; Weiss-

Penzias et al., 2007; Ewing et al., 2010). Studies applying chemical transport models (CTM) also show the transport of Asian pollutants to the Western U.S. However, they often suggest that only a small portion (<10%) of the Asian pollutants reaching the North American free troposphere actually descends into surface air (Yienger et al., 2000; Cooper et al., 2004a; L. Zhang et al., 2009). Also, these models further minimize the impacts of the transport on the vigorous episodic pollution events (Lin et al., 2010; Rastigejev et al., 2010). These studies which underestimate the modeled transport explain the disparity in terms of the limitation of the current model framework, such as coarse resolutions of the models, lack of numerical diffusion in the model physics, and limited understanding of meso-scale processes contributing to the exchange of pollutants between the boundary layer and the free troposphere. Although the models underestimate the magnitude of transported pollution, they still have the capability of simulating transport of pollutants, and can provide us information about the source distributions, the transport patterns, and duration time of pollutants in the atmosphere.

The primary goals of this study are i) to determine the source of an elevated O<sub>3</sub> episode using airborne measurements combined with multiple model platforms such as global-, regional-scale, and trajectory models, and ii) to help inform regional air quality management decisions by showing the methods to assess Asian pollution transport to the western U.S. for specific events when the natural atmospheric phenomena such as stratospheric intrusions are small. Here we focus on 30 May 2012, when high O<sub>3</sub> is observed offshore near the San Francisco Bay Area, CA as part of the Alpha Jet Atmospheric eXperiment (AJAX) project. In section 2, we describe the experimental design of AJAX measurements, models, reanalysis, and satellite data. Section 3 examines the local contribution to the observed O<sub>3</sub> concentration, as well as the influence of stratospheric intrusion on the delivery of high O<sub>3</sub> in this episode. We also demonstrate transport pathways of Asian pollution over the western U.S., including the high signature of CO over Asia, and this will confirm the mixing of Asian polluted air masses with stratospheric and upper tropospheric air. The potential impact of high O<sub>3</sub> aloft on surface O<sub>3</sub> in the CA boundary layer is also discussed. Finally, the summary and conclusions are described in Section 4.

## 2. Experimental design

### 2.1. Airborne instrumentation (Alpha Jet)

In situ measurements of O<sub>3</sub> were performed as part of the Alpha Jet Atmospheric eXperiment (AJAX). The aircraft is based at and operated from NASA Ames Research Center at Moffett Field, CA (37.42° N, 122.05° W). Scientific instrumentation is housed within one of two externally mounted wing pods. The aircraft instrumentation includes an O<sub>3</sub> monitor (described below), and a carbon dioxide (CO<sub>2</sub>) and methane (CH<sub>4</sub>) analyzer (Picarro Inc., model G2301-m). Further details on the airborne facility are presented in Hamill et al. (2016).

Measurements of O<sub>3</sub> mixing ratios were performed using a commercial O<sub>3</sub> monitor (2B Technologies Inc., model 205) based on ultraviolet (UV) absorption techniques and modified for flight capability. The dual-beam O<sub>3</sub> instrument uses two detection cells measuring the UV light intensity difference between O<sub>3</sub>-scrubbed air and un-scrubbed air. The O<sub>3</sub> monitor has undergone thorough instrument testing in the laboratory to determine the precision, linearity and overall accuracy. Calibration tests (ranging from 0 to 300 ppbv) were performed before and after flight using an O<sub>3</sub> calibration source (2B Technologies, model 306). The calibration factors for linearity offset and the zero offset (1.01 and -2.7 ppbv,

respectively) were applied to raw data during data processing. In situ O<sub>3</sub> measurements are taken every 2 s, and averaged to 10 s to improve precision. The typical overall uncertainty of the O<sub>3</sub> measurements is 3 ppbv. For more information, see Yates et al. (2013).

To compare offshore and inland ozone and greenhouse gas conditions and assess horizontal variability above and below boundary layers, the aircraft performed two consecutive vertical profiles (see Fig. 1). The takeoff time was 11:15 Pacific Daylight Time (PDT) (UTC time is PDT + 7 h) on 30 May 2012. The aircraft arrived on-station at Castle Airport (37.38°N, 120.56°W, inland) ~11:33 PDT and performed a descending spiral profile from 8.1 km to the lowest altitude ~ 0.07 km. Then the aircraft passed over offshore (37.2°N, 123.25°W, RAINS) arriving at 12:20 PDT with a descending spiral from 8.4 km to the lowest altitude ~ 0.03 km. Total duration for the flight was about 2 h, landing at Moffett field at around 13: 12 PDT.

## 2.2. Modeling analysis

In this study, we used three models including the global GEOS-Chem model and Lagrangian trajectory models (National Aeronautics and Space Administration Goddard Space Flight Center (NASA GSFC) back trajectory model, and the Weather Research and Forecasting–Stochastic Time Inverted Lagrangian Transport (WRF-STILT) model). The NASA GSFC back trajectory model was used for determining the origins (source regions) of air masses by tracing the position of mean wind trajectories. Mean wind trajectories may have difficulty in the PBL when the variability in observations is associated with a heterogeneous surface structure (i.e. mountains) and the surface condition is highly turbulent. The WRF-STILT model, one of the Lagrangian Particle Dispersion Models (LPDM), can overcome this limitation by simulating both advection and turbulence, and capturing the small scale heterogeneous structures

in the PBL. The WRF model provides meteorology input data to drive the STILT model.

### 2.2.1. GEOS-Chem model

To quantify the impact of North American pollution on airborne measurements evaluated during this study, the global/regional 3-D chemical transport model (CTM) GEOS-Chem (v9-01-03; <http://geos-chem.org/>) was applied to simulate emissions, atmospheric chemistry, transport, and deposition of O<sub>3</sub> and its precursor species. GEOS-Chem is driven by assimilated meteorological fields from the Goddard Earth Observing System (GEOS-5) of the National Aeronautics and Space Administration (NASA) Global Modeling Assimilation Office (GMAO) (Bey et al., 2001). The model was run in a regional nested-grid mode with a horizontal resolution of 0.5° × 0.67° (latitude × longitude) and 47 vertical hybrid sigma-pressure levels (including ~14 levels below 2 km) over North America. Transport of aerosol and gaseous species is calculated every 10 min in the model using the scheme described in Lin and Rood (1996). The planetary boundary layer (PBL) mixing scheme used in this study is based on Lin and McElroy (2010) and considers atmospheric instability conditions. Anthropogenic emissions in North America during this study were taken from the 2005 National Emissions Inventories (NEI) developed by the US Environmental Protection Agency (EPA). The model simulates biogenic volatile organic compound (VOC) emissions using the Model of Emissions of Gases and Aerosols from Nature (MEGAN v2.1) model. Daily wildfire and biomass burning emissions are taken from the version 3 Global Fire Emissions Database (GFED3) emission inventory. GEOS-Chem was also run in a tagged tracer mode in order to estimate the contribution of local emission sources in North America to the O<sub>3</sub> measured by AJAX. These model simulations tag the quantity of O<sub>3</sub> formed in the boundary layer over North America, and this tracer is then transported and is subject to

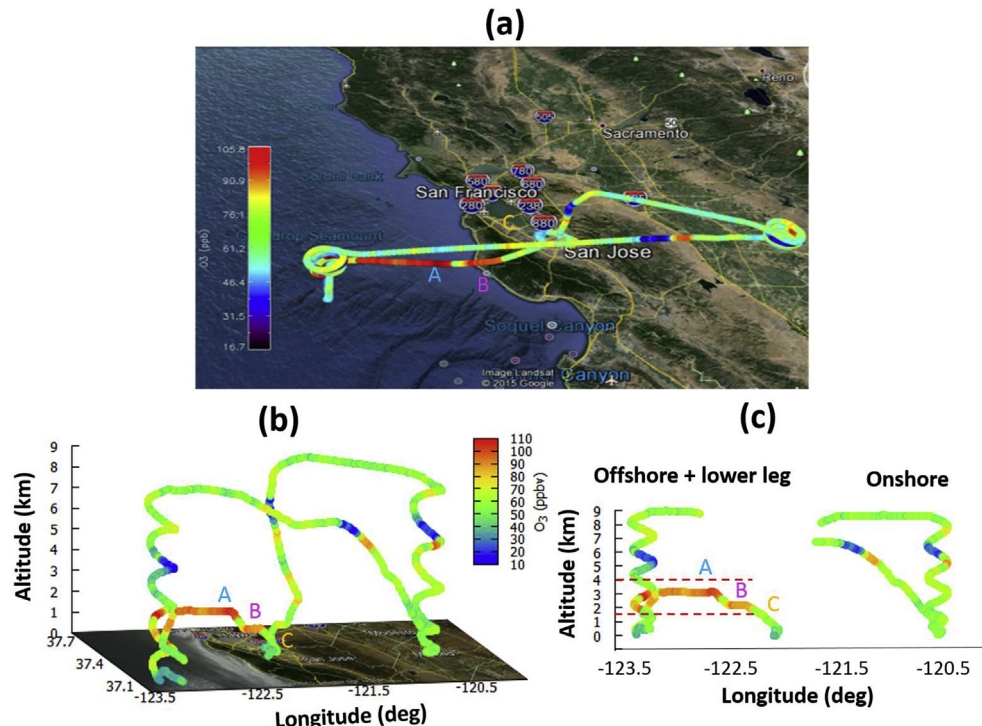


**Fig. 1.** (a) A map of AJAX flight track with ozone (O<sub>3</sub>) values plotted in Google™ Earth. (b) 3-D Vertical profile of O<sub>3</sub> mixing ratio (ppbv), and (c) the plane-view of vertical profile of O<sub>3</sub> offshore, lower leg and onshore measured by AJAX flight on 30 May 2012. The red dashed lines mark the altitudes between 1.5 and 4 km. (For interpretation of the references to colour in this figure legend, the reader is referred to the web version of this article.)

chemical production (only in the North American boundary layer) and loss processes (anywhere in the troposphere and stratosphere). The 3-hr dynamic boundary conditions for nested O<sub>3</sub> model runs are prescribed from global GEOS-Chem simulations with a 2° × 2.5° resolution.

### 2.2.2. WRF-STILT model

The Weather Research and Forecasting model combined with Stochastic Time Inverted Lagrangian Transport (WRF-STILT) model simulations were performed to identify local surface influence on the O<sub>3</sub> concentration at the sampled altitudes. The STILT model, based on the HYSPLIT model developed at NOAA's Air Resources Laboratory (Draxler and Hess, 1997, 1998), is described in Lin et al. (2003), while the WRF model is described in Skamarock and Klemp (2008) and extensively documented in Skamarock et al. (2008). Our WRF simulations consisted of two domains at 8 and 2.7 km resolution with two-way nesting over the west coast of the U.S. Time-averaged, mass coupled winds from the WRF model were used to improve mass conservation and the temporal representation of wind variation (Nehrkorn et al., 2010; Hegarty et al., 2013; Mallia et al., 2014). The native vertical levels within STILT were selected to closely match the WRF vertical levels to further improve mass continuity. WRF simulations were carried out from 27 May 2012 to 3 June 2012 with hourly output. The WRF physics options used for WRF-STILT simulation are shown in Supplementary Appendix Table S1. The STILT model is driven by meteorological fields produced by WRF using NCEP North American Regional Reanalysis (NARR, Mesinger et al., 2006) data which provides boundary conditions at a horizontal grid spacing of 32 km with 32 vertical levels every 3 h.

The STILT model is one of the Lagrangian Particle Dispersion Models (LPDM), which has been used for capturing subgrid scale transport (Stohl, 1998) and determining the surface impact on the concentration of conserved tracer at the observed sites (Ryall et al., 2001; Lin et al., 2003; Nehrkorn et al., 2010). This model expands traditional mean wind trajectory models by simulating both advection and turbulence in the trajectories of tracer particles in the PBL. A key advantage of the STILT model approach is the ability to identify the possible surface influence both backward and forward in time. Particles transported backward in time in STILT simulate the history of the air particles with their footprints. These footprints (or called sensitivity of mixing ratio (concentration) to surface fluxes) gives the concentration change at the starting point of the STILT run (receptor), given a unit flux from the ground surface [ppm/(μmol m<sup>-2</sup> s<sup>-1</sup>)]. In a similar way, particle transported forward in time provide a straightforward way for quantifying the impact of an emission source on the downstream concentrations with its possible influence on surface. Footprints (influence) are computed based on how many particles are found near the ground at a given location and how long they reside there, so that they can link the upstream or downstream influence to the concentration change at the receptor. Please see Lin et al. (2003), Nehrkorn et al. (2010), and Mallia et al. (2014), and the Supplementary Appendix for more detailed information for footprint or the surface influence.

### 2.2.3. NASA GSFC back-trajectory model

Back-trajectory calculations are performed using the NASA GSFC Trajectory Model. This model was developed by Schoeberl and Sparling (1995), and later modified by Wright et al. (2011). The parcel history (trajectory) X(t) is calculated by integration of the equation DX(t)/Dt=U(t), where X(t) is the location (longitude, latitude, and potential temperature) of the air parcel and U(t) is the three dimensional wind velocity (with diabatic heating rate as the vertical velocity). The trajectories are determined using the GMAO Modern Era Retrospective analysis for Research and Applications 2

(MERRA-2) reanalysis fields (Suarez and Bacmeister, 2015; Bosilovich et al., 2016). The MERRA-2 horizontal winds, temperatures, diabatic heating rates are reported at a horizontal resolution of 0.66° longitude by 0.5° latitude on 42 pressure levels spanning from 1 000 to 0.01 hPa, and 3-hourly time resolution. MERRA-2 is a NASA atmospheric reanalysis for the satellite era using the Goddard Earth Observing System Model, Version 5 (GEOS-5) with its Atmospheric Data Assimilation System (ADAS), version 5.12.4. See Bosilovich et al. (2011, 2016) for additional information regarding the MERRA and MERRA-2 reanalyses. All fields are vertically interpolated to a potential temperature grid, and are also interpolated linearly in time and space to the trajectory location at each time step of the trajectory integration. A fourth-order Runge-Kutta method is used to calculate trajectory motion, and it is calculated for every 28 min (i.e. fifty time steps per day).

For trajectory analysis, the west coast of the U.S. and northern California (CA) (36–42°N, 125–118°W) are used. Subset regions (37–37.5°N, 125–120°W) focused on locations closest to AJAX flight pathways are also considered. This selection not only covers the area that the AJAX aircraft measured, but also includes the surrounding areas, to capture as many back-trajectories as possible coming into CA. O<sub>3</sub> measurements in these regions are also important as the concentration can be affected both by transport or by local pollution (Huang et al., 2010; Lin et al., 2012a).

All trajectories are released at potential temperatures of 305, 308, 310, and 312 K (1.5–4 km in the mid-latitude). These levels are chosen for the back-trajectory calculation, specifically to determine the source of high O<sub>3</sub> offshore measured by AJAX. Back trajectories were also performed at lower potential temperatures (290, 295, 300 K, corresponding to 1–1.5 km) and higher potential temperature (315 K, 317 K, 320 K, 324 K, covering 4–6 km in the mid-latitude) to track the sources of the parcels above and below the O<sub>3</sub> lamina at 3 km both offshore and inland. For each back-trajectory track, calculations are started from a regular longitude-latitude grid with spacing of 0.625° by 0.5° covering the region of California at each potential temperature level, resulting in 1716 (156 × 11) (subset: 198 (= 18 × 11)) trajectories for this flight. Trajectories are computed backward for 10 days. The typical timescale for air parcels to come across the Pacific Ocean during boreal spring is longer than a week, which is the nominal time of transit during boreal winter (Roca et al., 2005; Moncrieff et al., 2007; Ryoo et al., 2015). Ryoo et al. (2015) reports that there are no significant differences between trajectory results using different meteorological fields such as National Centers for Environmental Predictions (NCEP) (Kalnay et al., 1996) or European Centre for Medium-Range Weather Forecasts (ECMWF) (Simmons et al., 2007) or MERRA reanalysis data over the west coast of the U.S. Trajectories using MERRA and MERRA-2 show only minor differences, but MERRA-2 carries improved information, especially in the upper troposphere and the lower stratosphere due to the improved accuracy in the input of satellite measurements (see Supplementary Appendix. Fig. S4).

### 2.2.4. MERRA-2 assimilated O<sub>3</sub> and NOAA interpolated daily outgoing longwave radiation (OLR)

Compared to native MERRA O<sub>3</sub>, which is produced based on coarser resolution data from Solar Backscattered Ultra Violet (SBUV) instruments, MERRA-2 assimilated O<sub>3</sub> fields are produced based on total column O<sub>3</sub> observational data from the Ozone Monitoring Instrument (OMI; Levelt et al., 2006) with Microwave Limb Sounder (MLS; Waters et al., 2006) O<sub>3</sub> profiles at 0.625° × 0.5° (about 50 km) horizontal resolution. The O<sub>3</sub> assimilation system used in MERRA-2 is described in more detail in Wargan et al. (2015). It is known that MERRA-2 can realistically reproduce O<sub>3</sub> observations in the upper troposphere and lower stratosphere (UT/

LS) and above, due to strongest data constraints in the higher altitudes, but it underestimates the actual O<sub>3</sub> in mid-to lower troposphere, due to lack of emissions and simplified photochemistry in the mid-to lower troposphere (Wargan et al., 2015; Ott et al., 2016). Considering all this, MERRA-2 O<sub>3</sub> fields can be expected to provide a realistic estimate of mixing ratios within stratospheric intrusion layers, but will weakly represent observations in air masses dominated by surface emissions. The comparison between MERRA and MERRA-2 shows that their difference is considerable in the upper troposphere and the stratosphere (up to 100 ppbv) in our study location (see Supplementary Appendix Figs. S2 and S3). We compare our aircraft O<sub>3</sub> results with assimilated O<sub>3</sub> fields produced by MERRA-2 in Section 3.3.2.

Outgoing longwave radiation (OLR) is used as a simple proxy of deep convection. The OLR data used are the NOAA spatially and temporally interpolated OLR (Liebmann and Smith, 1996), obtained from the NOAA Cooperative Institute for Research in Environmental Sciences (CIRES) Climate Diagnostics Center (CDC; information available online at <http://www.cdc.noaa.gov/>). The temporal resolution is daily, and horizontal resolution is longitude 2.5° by latitude 2.5°.

### 3. Results and implications

#### 3.1. Local sources

##### 3.1.1. Comparison of AJAX observations with GEOS-Chem model simulation

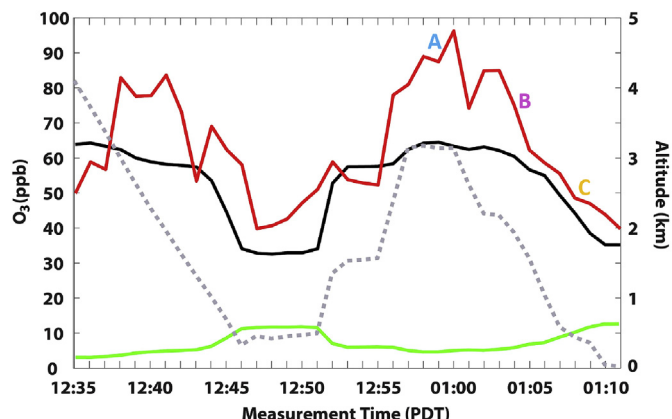
Fig. 1 illustrates the 30 May 2012 AJAX flight track showing O<sub>3</sub> mixing ratios and vertical distributions. The locations of A, B, C are chosen to see O<sub>3</sub> at different altitudes close to the coast line. It is interesting to note that higher O<sub>3</sub> (>80 ppbv) is observed around and below 3 km offshore than anywhere onshore. Onshore, relatively high O<sub>3</sub> and its gradient has been observed around 5–7 km, but this is not as high as values observed offshore around 3 km (see Fig. 1b and c). High O<sub>3</sub> mixing ratios observed around 6–7 km are commonly attributed to PV and high O<sub>3</sub> from the lower stratosphere into the mid-troposphere (Langford et al., 2009, 2012; Lin et al., 2012b; Yates et al., 2013). High gradients observed in the lower altitudes around 3 km, however, the processes and sources leading to enhanced O<sub>3</sub> are not yet well understood.

Fig. 2 shows the time series of 1 min averaged measured O<sub>3</sub>, total O<sub>3</sub> simulated from GEOS-Chem, and GEOS-Chem North America boundary layer tagged tracer sampled along a portion of the flight track. Simulated O<sub>3</sub> values are sampled from the model using predictions from the time-step and horizontal and vertical grid corresponding to the location and timing of AJAX measurements. There is a fairly good agreement between AJAX O<sub>3</sub> and the total GEOS-Chem simulated O<sub>3</sub>. Although the magnitude of modeled O<sub>3</sub> is smaller than AJAX measured O<sub>3</sub> in the lamina between 2 and 4 km, the peaks and patterns of both modeled and observed O<sub>3</sub> are well correlated ( $R = 0.74$ , Normalized Mean Bias = -18.2%). GEOS-Chem tends to underestimate the measured O<sub>3</sub> during the times of strong stratospheric intrusions, as shown in previous studies (Zhang et al., 2014). Overall, the GEOS-Chem simulations during this study predict that local sources play a minimal role in O<sub>3</sub> contribution to that measured by AJAX off the coast of northern California (~1–20% of total simulated O<sub>3</sub>), and this suggests that other sources are primarily responsible for the observed high O<sub>3</sub> lamina measured by AJAX.

#### 3.2. Stratospheric intrusion into troposphere

##### 3.2.1. Meteorological features

It has been recognized that stratospheric intrusions are one of



**Fig. 2.** Time series of 1 min averaged AJAX O<sub>3</sub> (red), total O<sub>3</sub> simulated from GEOS-Chem (black), and GEOS-Chem simulated local North American O<sub>3</sub> (green) on 30 May 2012 sampled along a portion of the flight track from 12:35 to 13:10 PDT (time is PDT + 7 h). Location A refers to 37.15 °N, 122.65 °W at 3 km; B to 37.21 °N, 122.30 °W at 1.8 km; C to 37.27 °N, 122.10 °W at 0.5 km, as depicted in Fig. 1. The gray line represents AJAX altitude (km). The O<sub>3</sub> simulated from GEOS-Chem are calculated along the AJAX flight path which passed through 2 different latitude (36.75–37.75 °N) and 3 different longitude (121.667–123.667 °W) model grids with more than 15 vertical model grids. (For interpretation of the references to colour in this figure legend, the reader is referred to the web version of this article.)

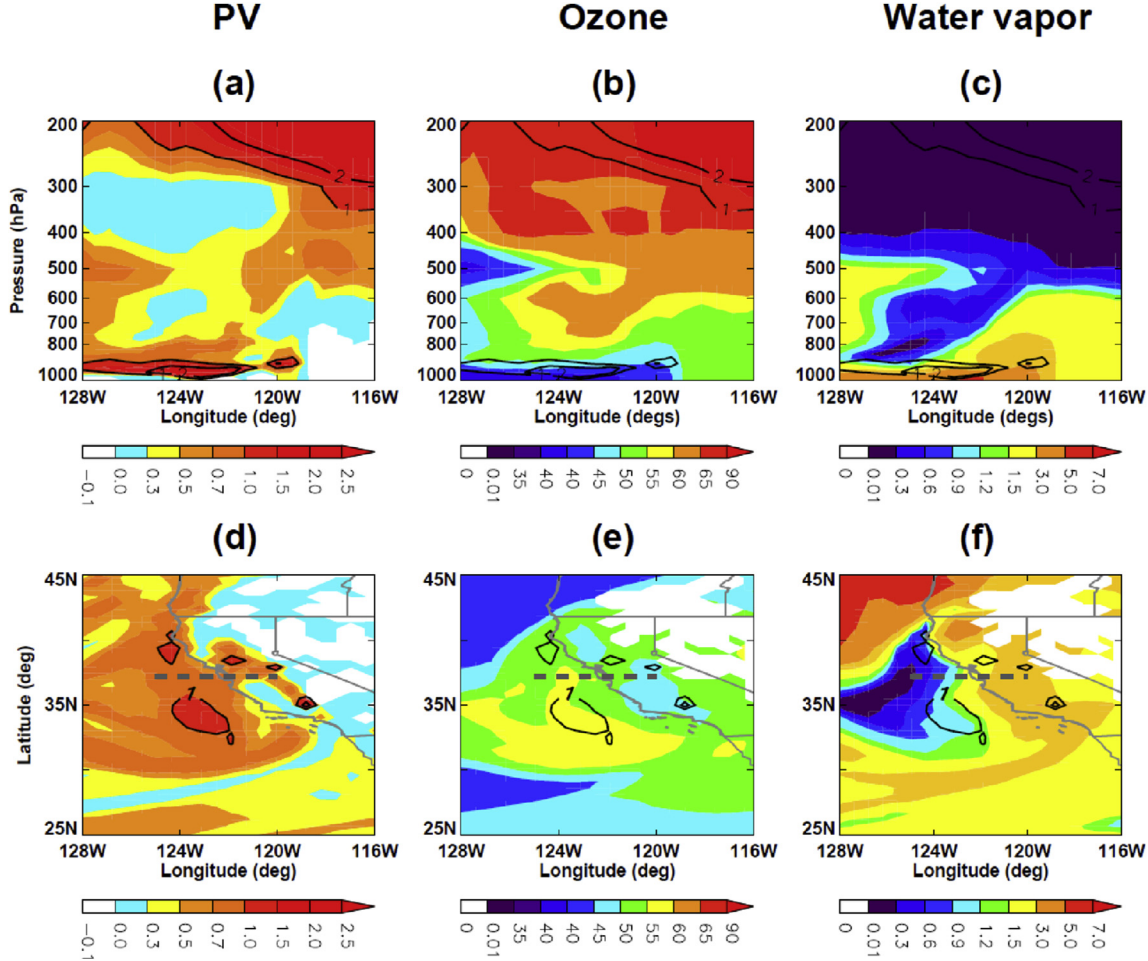
the major contributors to elevated O<sub>3</sub> in the lower troposphere of North America during the spring and winter months (Bourqui and Trepander, 2010; Chung and Dann, 1985; Cooper et al., 2004b, 2005, 2011; Ambrose et al., 2011; Yates et al., 2013). To determine if the stratospheric impact on O<sub>3</sub> measured by AJAX on 30 May 30, 2012 is significant, we first examine the atmospheric conditions such as temperature, wind, and PV fields. PV is a conservative tracer under adiabatic conditions and is typically much larger in the stratosphere than troposphere. In general, the dynamic tropopause is defined when PV is equal to 1.5 PVU (1 PVU =  $10^{-6} \text{ m}^2 \text{s}^{-1} \text{ K kg}^{-1}$ ) or 2 PVU, so large PV values at high altitudes are regarded to be linked to the stratosphere.

Fig. 3 shows that high O<sub>3</sub> may be partially coming from the upper troposphere and lower stratosphere (UT/LS) through intrusions. A large region of increased ozone (Fig. 3b) has been drawn down to ~700 hPa, and a relatively weak tongue of PV descending from the UT/LS with a separate region of high PV (>1 PVU) seen at low altitudes highlights likely stratospheric influence. However, we cannot say that these air masses are exclusively transported from the UT/LS because the air is not completely dry (i.e.  $q$  is not very low). Furthermore, the magnitude of PV in the flight region is still small (0.5–1 PVU) (see Fig. 3a and d). Thus, we suggest that this moist air with modest PV values is the result of sufficient turbulent mixing (Shapiro, 1980) between upper- and lower-level air.

If these features are not due to transport of air from the stratosphere, how can PV be so large at near the surface (1 000–800 hPa), and where was that high PV region formed? The short answer for the question appears to lie in understanding the role of diabatic heating on PV formation. The diabatic heating effect in lower altitudes is known to be a dominant factor that produces low-level PV and moistens the air (Hoskins et al., 1985; Lamarque and Hess, 1994). According to Hoskins et al. (1985), PV can be modified by diabatic heating/cooling processes:

$$\frac{D}{DT} PV = \frac{1}{\rho} \eta \cdot \nabla (DHR) \approx \frac{1}{\rho} \eta_Z \cdot \frac{\partial}{\partial Z} (DHR) \quad (1)$$

Where  $D/Dt$  denotes the material derivative,  $\eta$  is absolute vorticity vector, and  $DHR$  is the diabatic heating rate. Fig. 4 demonstrates



**Fig. 3.** (Top) Longitude-Height vertical cross section averaged over 36–37.5 °N, and (Bottom) Longitude-Latitude cross section at 825 hPa of (a, d) Potential vorticity (PV, in PVU), (b, e) O<sub>3</sub> (in ppbv), and (c, f) specific humidity ( $q$ , in g/kg) on 30 May 2012 at 18 UTC obtained from MERRA-2 reanalysis data. The white area represents the data affected by mountainous area. The black contours refer to PV of 1, 2 PVU (1 PVU =  $10^{-6}$  K m<sup>2</sup> Kg<sup>-1</sup> s<sup>-1</sup>), and the dashed dark-gray lines refer to the latitude of 37.2 °N closest to the flight track.

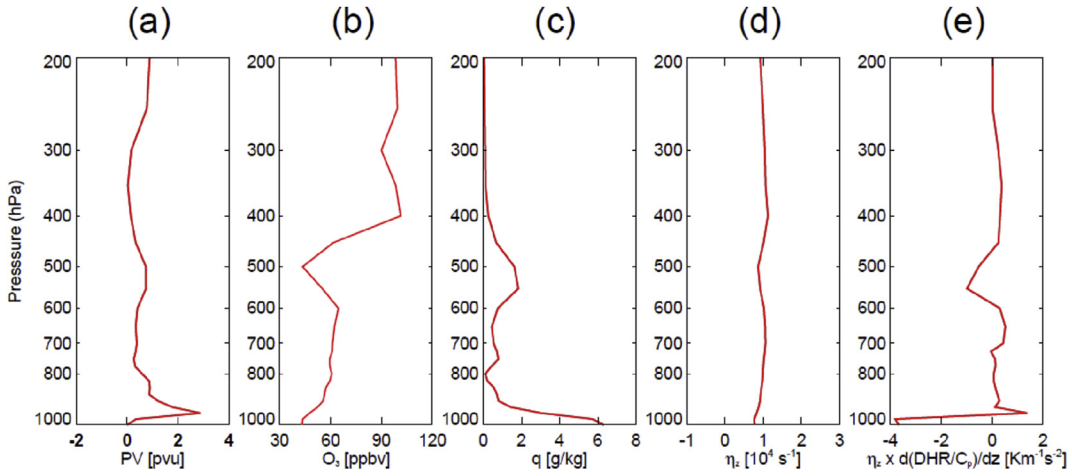


**Fig. 4.** Vertical profiles of (a) PV, (b) O<sub>3</sub> mixing ratio, (c) specific humidity ( $q$ ), (d) vertical vorticity, and (e) vertical vorticity multiplied by  $d(DHR/C_p)/dz$  averaged over 37–37.5 °N, 125–120 °W on 30 May 2012 at 18 UTC computed using MERRA-2 reanalysis data.

how PV at a lower altitude is modified by absolute vorticity (curl of wind vector) and the vertical gradient of diabatic heating. The peak of PV values in the lower altitude between 1 000 and 800 hPa matches well with the peak of the combination of absolute vorticity

and the vertical gradient of diabatic heating rate ( $\partial(DHR)/\partial Z$ ) (see Fig. 4a, d, 4e). The vertical profile of  $q$  also shows that the air in the low altitude is not as dry as the high altitude (Fig. 4c). From these figures and the PV formation process in the low altitude (Eqn (1)),

we now see that the atmospheric variables such as PV, O<sub>3</sub>, and  $q$  on 30 May 2012 were more influenced by the diabatic heating processes through mixing of airs, rather than stratospheric intrusion.

### 3.3. Long-range transport

#### 3.3.1. Back-trajectory model simulations

From sections 3.1–3.2, we demonstrate that local sources and stratospheric intrusions can only partially explain the high O<sub>3</sub> detected by AJAX on 30 May 2012. Long-range transport is known as an important process to cause pollutant transport to the U.S. across the Pacific (e.g., Lin et al., 2012a). Such pollution is observed by recent satellite images. Fig. 5a shows MOPITT (Measurement of Pollution In The Troposphere) column carbon monoxide (CO) averaged over 21–30 May 2012, depicting that much pollution over Northern China is emitted from combustion and other anthropogenic sources during the days prior to the AJAX flight.

In order to determine the impact of long-range transport on high O<sub>3</sub> concentration observed by AJAX, we perform a back-trajectory analysis. Fig. 5 shows the spatial and temporal evolution of NASA GSFC back-trajectories starting from California (36°N–42°N, 125°W–118°W) at 18 UTC on 30 May 2012 for about 10 days. The starting points of the colored lines represent the locations similar to where AJAX observed (37°–37.5°N, 124°–120°W,

total 18 trajectories), and the symbols represent the parcel positions at days –3, –6, and –9. The horizontal and vertical evolutions of trajectories clearly show that air masses come from different locations and altitudes. Among them, the majority of air parcels are transported from northern Asia across the Pacific (Fig. 5b). The shaded areas in panel (b) of Fig. 5 indicate biomass burning area obtained from the Global Fire Emission Database (GFED, van der Werf et al., 2010; Giglio et al., 2013), suggesting that Russian wildfire can be one of the sources of O<sub>3</sub> formation or precursor generation. Furthermore, the low OLR (less than 190 W m<sup>–2</sup>), which is typically associated with deep atmospheric convective updraft, is found over the northern Asia and western Pacific around day –10 to –9. This can trigger uplifting of the polluted air parcel from the areas over Russia and northern China to the free troposphere.

The time series of trajectories shown in Fig. 5c shows that the air masses are “mixed” with each other during the process of transport. To explore how the mixing of air masses from different sources can be identified by an objective diagnostic, and whether such a diagnostic can be used as an objective predictor of mixture of air mass from different origins, we use Q as a measure of mixing of air parcels in the large-scale flow:

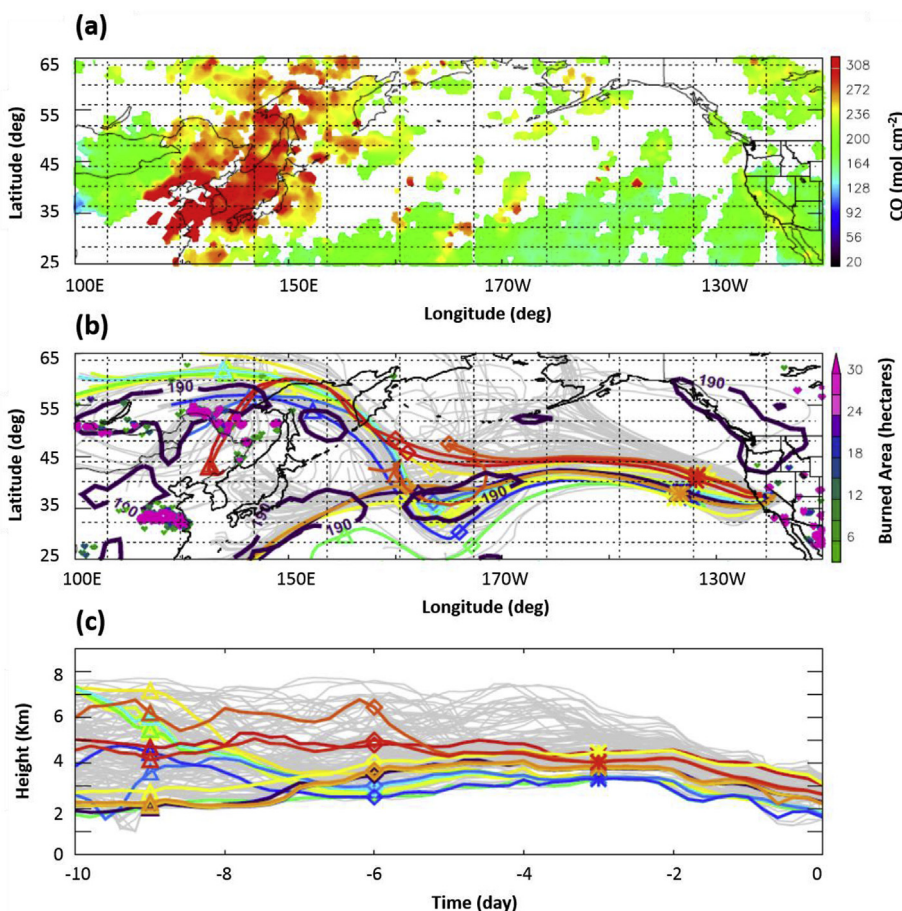


**Fig. 5.** (a) Daytime column CO averaged over 21–30 May 2012 obtained from MOPITT data, (b) horizontal pathways, and (c) vertical evolution of 10 day back-trajectories releasing at 305, 308, 310, and 312 K (1.5–4 km) using MERRA-2 reanalysis data coming to California (36–42°N, 125–118°W on day 0 (30 May 2012 at 18 UTC)). Different colors of the trajectories represent the individual trajectories starting at locations closest to AJAX flight path (37–37.5°N, 124–120°W) ending in different regions. The line colors closer to red (blue) signify the trajectories originating further north and higher altitude (south and lower altitude). The symbols represent the parcel locations at –3, –6, and –9 days. The colored regions in (b) represent burned area obtained from GFED. The purple contours are low OLR (190 W m<sup>–2</sup>) at day –9, which is used as a proxy of deep convection. (For interpretation of the references to colour in this figure legend, the reader is referred to the web version of this article.)

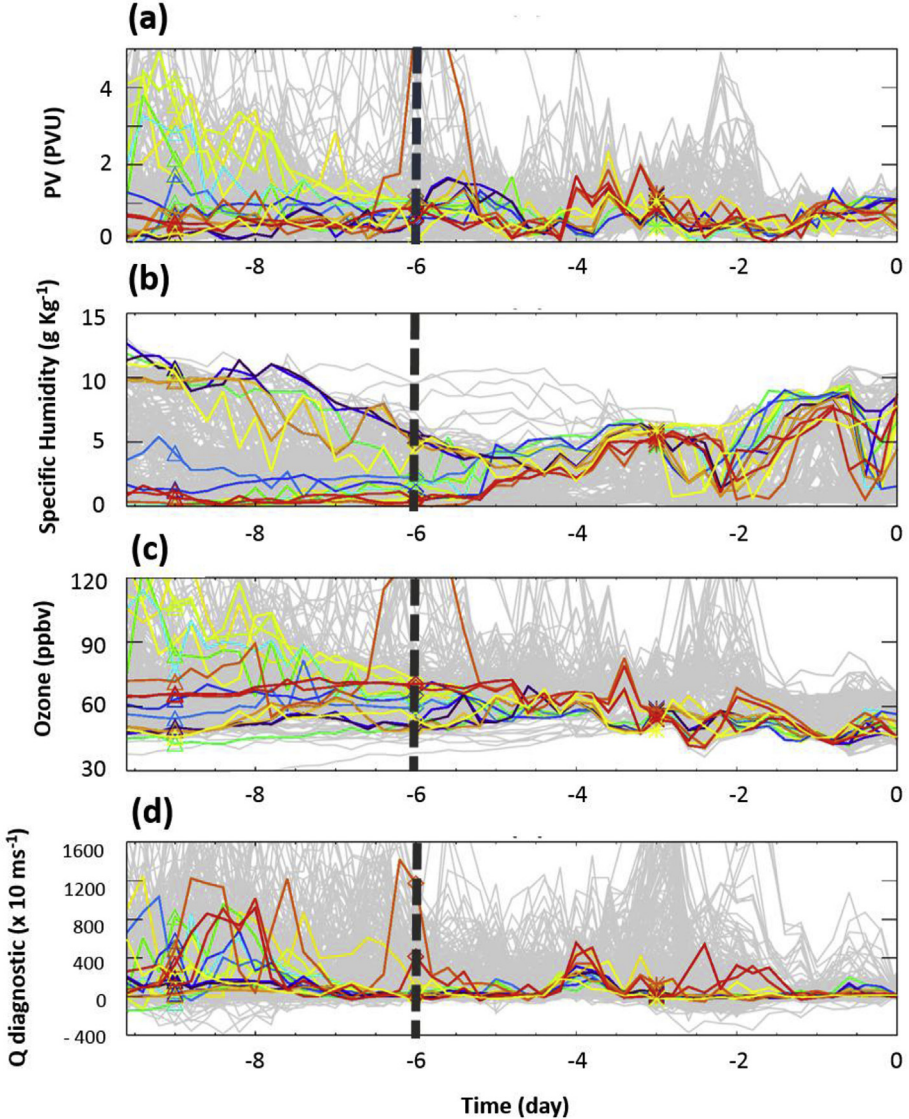


**Fig. 6.** The same as Fig. 5(c) except for the time series of  $\text{O}_3$ , PV, specific humidity, and Q diagnostic. The line colors closer to red (blue) signify the trajectories originating further north and higher altitude (south and lower altitude). The starting position of each colored trajectory is marked as the same colors in Fig. 5. The dashed vertical lines show the each value at day -6. (For interpretation of the references to colour in this figure legend, the reader is referred to the web version of this article.)

$$Q = \frac{1}{2} \left( \frac{1}{\cos \varphi} \frac{\partial u}{\partial \lambda} - v \tan \varphi \right)^2 + \frac{1}{2} \left( \frac{\partial v}{\partial \varphi} \right)^2 + \frac{\partial u}{\partial \varphi} \left( \frac{1}{\cos \varphi} \frac{\partial v}{\partial \lambda} + u \tan \varphi \right) \quad (2)$$

Where  $\lambda$  and  $\varphi$  are longitude and latitude, respectively (Haynes, 1990; Fairlie et al., 2007). Positive  $Q$  means the fluid elements are stretched, so that there is efficient mixing of air, and this is found to be associated with the regions of Rossby wave breaking,<sup>1</sup> where efficient mixing between air masses happens. Negative  $Q$ , on the other hand, indicates that rotation of fluid is dominant, so air

masses do not tend to be stretched or mixed and this is associated with non-Rossby wave breaking events.

Fig. 6 shows (a) PV, (b) specific humidity ( $q$ ), (c)  $\text{O}_3$  mixing ratios, and (d) Q diagnostic computed along the trajectories obtained from the nearest location to MERRA-2  $\text{O}_3$  at each grid point for 30 May 2012. Note that, during the period of the back-trajectories from the AJAX flight sites, high positive  $Q$  values (larger than 600) are detected between day -6 and day -10, showing that there is efficient mixing among parcels during the transport across the Pacific; some of parcels are from Asia, and some of them from the stratosphere and the upper troposphere, and they are mixed together in the course of the transport. These large positive  $Q$  values in the course of back-trajectories indicate that there are significant sources in Asia across the Pacific, and they are transported through strong wind across the Pacific over several days, contributing the high  $\text{O}_3$  in the altitude range between the free troposphere and the boundary layer observed by AJAX over northern California. As a result of this mixing, for example, after a big jump in Q diagnostic values at day -6, dry air with low  $q$  originating from the UT/LS gets

<sup>1</sup> Rossby waves, also known as planetary waves, are long horizontal wavelength (>2000 km) oscillations in the westerlies that predominantly occur in the upper troposphere and the lower stratosphere. In the Northern Hemisphere (NH) winter, Rossby waves can grow to large amplitudes when winds are westerlies, but eventually break with irreversible mixing of potential vorticity when the winds are not westerlies and other wave growth conditions are not satisfied.

moist around day  $-4$  to  $-6$  (red), while PV and  $O_3$  originating from UT/LS get smaller at this time. Thus, Fig. 6 demonstrates that the air coming to the western U.S. is a mixture from many different sources.

### 3.3.2. Comparison with a stratospheric intrusion dominant case: 14 May 2012

Approximately two weeks before the case study discussed here, a large stratospheric intrusion event was identified by both observations and the Realtime Air Quality Model System (RAQMS) model (Yates et al., 2013) over California. Here we contrast how the 30 May 2012 enhancement is due to a combination of processes, rather than solely a stratospheric intrusion.

Fig. 7 shows the vertical distributions of  $O_3$  onshore and offshore, and the scatter plots of  $O_3$ , carbon dioxide ( $CO_2$ ), and water vapor ( $H_2O$ ) measured by AJAX during the 14 May 2012 and the 30 May 2012 flights, respectively. For the clear stratospheric intrusion case (14 May 2012, panel e), high  $O_3$  is observed where low  $H_2O$  ( $<0.01\text{ %v}$ ) is observed. This indirectly indicates that  $O_3$  mainly came from the dry, but  $O_3$ -rich stratosphere through intrusions. The vertical distribution of other greenhouse gases such as  $CO_2$ , methane ( $CH_4$ ) and  $H_2O$  show relatively no variation except for the low altitudes. In contrast, for 30 May 2012 (Fig. 8g), high  $O_3$  observed offshore in relatively low altitude (2–4 km) and the vertical profiles of  $CO_2$ ,  $CH_4$ , and  $H_2O$  also show more variation than those in the 14 May case (see Supplement Appendix, Fig. S1). Note that this strong  $O_3$  enhancement between 1.5 and 4 km (850–650 hPa) for 30 May case was not captured by MERRA-2  $O_3$  (see Fig. 4b). For the 14 May case, there is strong anti-correlation between  $O_3$  and  $H_2O$ . The scatter plots between  $CO_2$  and  $H_2O$  also show less variation in  $CO_2$  offshore for the 14 May case compared to

those for the 30 May case. This demonstrates that greenhouse gases and  $O_3$  observed for the 30 May 2012 case come from the combination of sources.

For further characterization of these features, the vertical cross sections of PV averaged over 121–123°W on 14 May 2012 and 30 May 2012 at 18 UTC, and their 5-day back trajectory pathways along with  $O_3$  and Q diagnostic are shown in Fig. 8. There is a stronger stratospheric intrusion over 30–40°N for 14 May 2012 compared to 30 May 2012 especially the strength of penetration of PV from the high altitude to the lower altitude (see Fig. 8a and b). The horizontal map of the cross section at 500 hPa (5–6 km) shows that there are strong PV tongues, penetrating from the stratosphere into the lower troposphere for both 14 May and 30 May cases. The big difference is that how deep the penetration is to the mid and lower levels. The stronger penetration into the mid-level (~500 hPa) was clearly found in 14 May case, where the AJAX flight passed through (Fig. 8c), but not in the 30 May 2012 case (Fig. 8d). Moreover, the transport patterns look quite different. Fig. 8c–f shows that the intrusion-dominated air masses are transported along the southerly path near the eastern Pacific, not far across the Pacific. Note that there is relatively weak mixing (small Q) around day  $-4(\alpha)$  on 14 May case while strong mixing (large Q) occurs around day  $-4(\alpha')$  for the 30 May case, with slightly increased amounts of  $O_3$  for 30 May case. Interestingly, the  $O_3$  peak is shown around day  $-0.5(\beta)$  after large mixing (large Q) on 14 May, indicating that there is direct influence from the  $O_3$ -rich region of the upper troposphere and the lower stratosphere throughout the intrusion, given no particular local  $O_3$  source off the coast. This indicates that direct transport of stratospheric air and its mixing near day 0 was a primary source of the high  $O_3$  value (Fig. 8i and k) around days  $-1$  and  $0$  for the 14 May case. Compared to this, the 30 May 2012 case

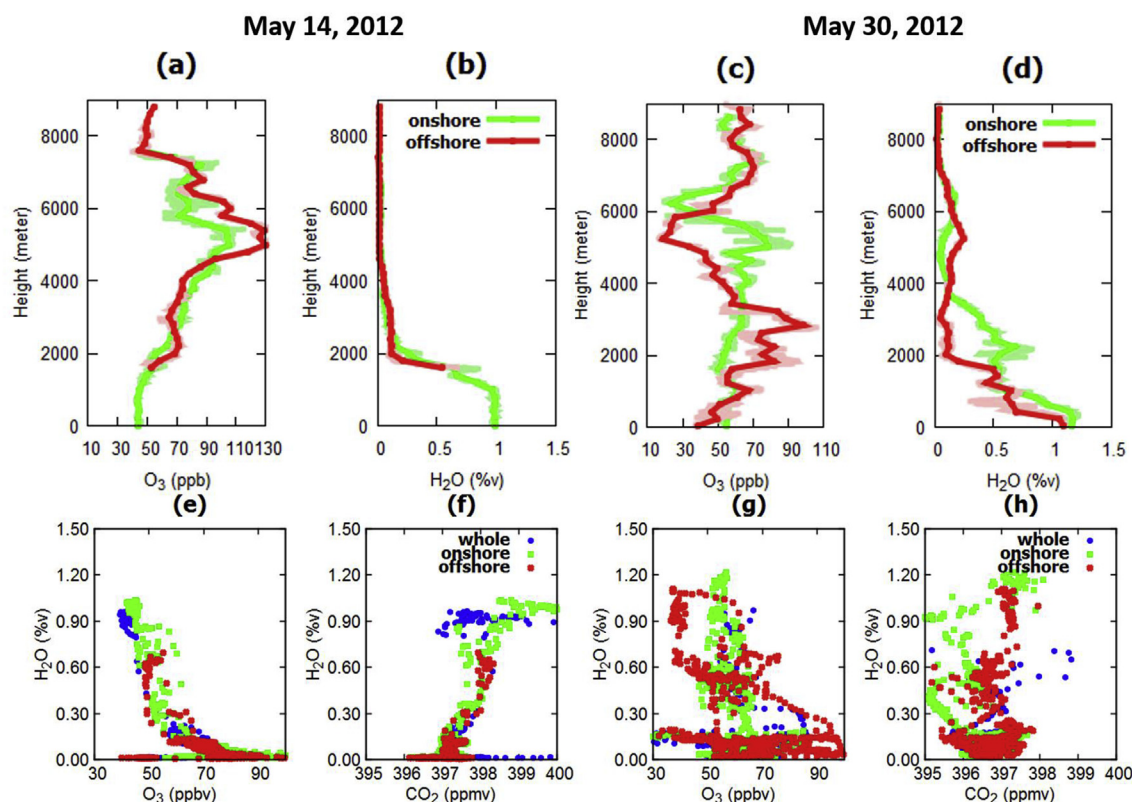


**Fig. 7.** (a–d) Vertical onshore (green) and offshore (red) profiles of  $O_3$  [ppbv] and  $H_2O$  [%v], (e–h) scatter diagrams of  $O_3$  and  $CO_2$  with  $H_2O$  during (left: a, b, e, f) 14 May 2012 case and (right: c, d, g, h) 30 May 2012 case. The red and green (pink and light-green) lines in (a–d) are vertical profiles averaged by every 200 (25) meters for heights for each gas, respectively. (For interpretation of the references to colour in this figure legend, the reader is referred to the web version of this article.)

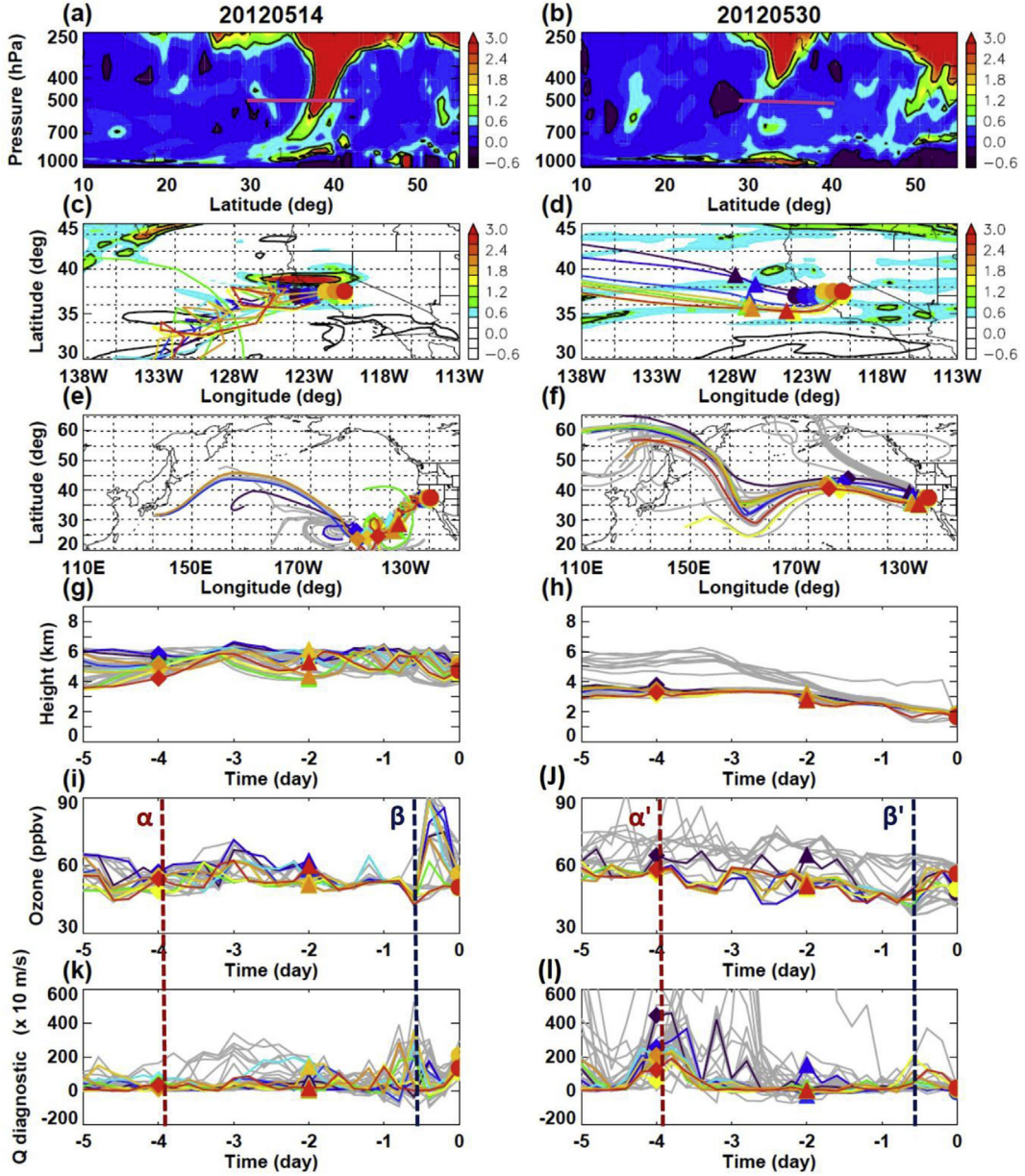


**Fig. 8.** (a, b) The latitude-pressure cross-section of MERRA-2 PV, (c, d) the back-trajectories near the AJAX flight lines overlaid with PV at 500 hPa (from the solid pink lines from (a, b)), (e, f) 9.4 day back-trajectories coming to California ( $36\text{--}42^\circ\text{N}$ ,  $125\text{--}120^\circ\text{W}$ ), releasing at (left) 315 K on 14 May 2012, and (right) 305 K on 30 May 2012 at 18 UTC, (g, h) vertical motions of the back-trajectories to AJAX flight path ( $37\text{--}37.5^\circ\text{N}$ ,  $124\text{--}120^\circ\text{W}$ ) ending in different regions. The trajectory colors represent the individual trajectories starting at locations closest to AJAX flight path ( $37\text{--}37.5^\circ\text{N}$ ,  $124\text{--}120^\circ\text{W}$ ) ending in different regions. The trajectory colors closer to red (blue) signify the trajectories originating further north (south). Dashed lines  $\alpha$ ,  $\beta$  ( $\alpha'$ ,  $\beta'$ ) represent O<sub>3</sub> and Q diagnostic around day  $-4$  and day  $-0.5$  for both 14 May 2012 and 30 May 2012, respectively. (For interpretation of the references to colour in this figure legend, the reader is referred to the web version of this article.)

shows less O<sub>3</sub> with somewhat moderate mixing (small Q) around day 0.5 ( $\beta'$ ), which implies that mixtures of air from multiple sources through mixing earlier ( $>\text{day } -4$ ,  $\alpha'$ ) lead to O<sub>3</sub> values at the time of observation (day 0).

The analysis presented here shows that the 30 May 2012 case has more complex patterns, suggesting that O<sub>3</sub> has multiple sources with the mixture of air, while the 14 May 2012 case has simpler patterns, identifying that O<sub>3</sub> has a stratospheric origin (Fig. 8i–l). Although high PV signatures in the mid-to high altitudes are clearly linked to stratospheric intrusions, especially in the eastern Pacific (Waugh, 2005; Ryoo et al., 2008), 30 May 2012 case shows that there is more contribution of long-range transport than pure stratospheric intrusion. These relatively weak PV signatures and

the horizontal transport pathways from Asia clearly indicate that complicated processes are involved in this case.

Fig. 9 summarizes where the air masses coming to CA originated and how much the different source regions contribute to the O<sub>3</sub> captured by the trajectories. It also shows how the observed O<sub>3</sub> is different from the MERRA-2 assimilated O<sub>3</sub>. The trajectories are classified, using their altitudes, as originating from the upper troposphere and the lower stratosphere (UT/LS, if trajectory at day  $-10$  comes from above 8 km), mid- (MT, if trajectory at day  $-10$  comes from between 3 and 8 km), and lower troposphere (LT, if trajectory at day  $-10$  comes from below 3 km). Panel (a) was computed from the form  $n_i/\sum_{i=1}^3 n_i$  which is the ratio of the number of trajectories ( $n_i$ ) in each group ( $i$ ) to the total number of

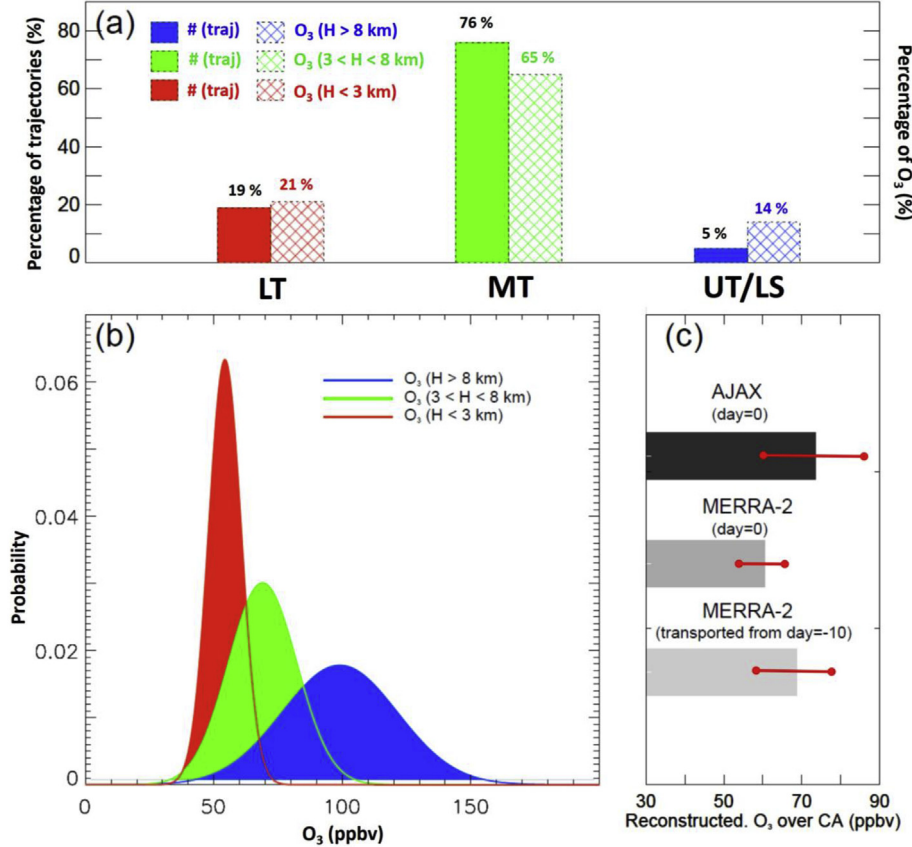


**Fig. 9.** (a) The percentage of back-trajectories (solid bar) and percentage of O<sub>3</sub> (hatched bar) from the different source regions: i) lower troposphere (LT) in red, ii) mid troposphere (MT) in green, and iii) upper troposphere/lower stratosphere (UT/LS) in blue, (b) Probability density function (PDF) of the O<sub>3</sub> mixing ratio of different sources (LT, MT, UT/LS) at the end of back trajectories (day -10) coming to California (37–37.5 °N, 125–120 °W) at 1–6 km) on 30 May 2012. (c) (top) AJAX-measured O<sub>3</sub>, (middle) MERRA-2 assimilated O<sub>3</sub>, (bottom) Reconstructed O<sub>3</sub> from the trajectories at day -10 to the nearby region of California offshore closest to AJAX flight paths (37–37.5 °N, 124–122 °W at 1.5–4 km) on 30 May 2012. The horizontal red line in each bar in (c) stands for its standard deviation. (For interpretation of the references to colour in this figure legend, the reader is referred to the web version of this article.)

trajectories arriving into the source regions. Panel (b) was obtained from the mean and standard deviation of the each classified trajectory group, and panel (c) was obtained from the equally averaged O<sub>3</sub> values, i.e.  $\overline{O_3} / \sum_{i=1}^3 \overline{O_{3i}}$  which is the ratio of the mean O<sub>3</sub> ( $\overline{O_{3i}}$ ) in each group ( $i = 1, 2, 3$ ) to the sum of the mean O<sub>3</sub> coming from all source regions. The proportion of trajectories coming from UT/LS is lower (5%) compared to that from the MT (76%) and the LT (19%), and the O<sub>3</sub> mixing ratio in the air masses coming from UT/LS is still lower (14%), compared to those from the MT and LT (65%, 21% respectively) (Fig. 9a). The probability density function (PDF) plots (Fig. 9b) show that the O<sub>3</sub> mixing ratio coming from UT/LS has not only a large mean, but also a large standard deviation, while O<sub>3</sub> coming from LT has both a small mean with a small standard deviation. The air mass coming from LT appears to be mostly coming from Asia (Fig. 5), and it accounts for about 20% of the total O<sub>3</sub> mixing ratio in this particular case. The contribution of O<sub>3</sub> mixing ratio from MT was highest, reaching about 65%, although its contribution is expected to vary depending on individual cases because they are affected by both LT and UT/LS. Fig. 9c summarizes the measured O<sub>3</sub> by AJAX between 1.5 and 4 km offshore at day 0 (18 UTC, 30 May 2012), MERRA-2 O<sub>3</sub> between 1.5 and 4 km at day 0, and transported O<sub>3</sub> computed using the relative percentage of trajectories from day -10 multiplied by its mean values, coming to the altitude between 1.5 and 4 km at day 0. The mean O<sub>3</sub> measured by AJAX is  $72.3 \pm 14.4$  ppbv while MERRA-2 mean O<sub>3</sub> is  $60.4 \pm 5.3$  ppbv. The reconstructed O<sub>3</sub> by trajectories transported from day -10 days to day 0 is  $68.9 \pm 10.1$  ppbv, which better

matches with the measured O<sub>3</sub>, but still underestimate the measured O<sub>3</sub> enhancement by 3 ppbv. The sensitivity of O<sub>3</sub> depending on the selection of regions (e.g. broad regions (36–42 °N, 125–118 °W) versus narrow regions of CA along with AJAX flight paths (37–37.5 °N, 124–120 °W)) was about  $\pm 5$  ppbv, but MERRA-2 consistently underestimates the actual O<sub>3</sub> measured by AJAX no matter where we choose. Overall, MERRA-2 O<sub>3</sub> tends to underestimate the measured O<sub>3</sub> enhancement in the layer of 1.5–4 km, especially the O<sub>3</sub> lamina offshore, by approximately 3–12 ppbv. This may be because of the relatively coarse resolution of MERRA-2 data compared to the observation, and the coarse footprint of the MLS observations (approximately 200–300 km), diminishing its capability to capture fine-scale laminar features of O<sub>3</sub> affected by intrusion, surface emission, and long-range transport. Fig. 9 also shows that the contribution of long-range transport and Asian pollution on the western U.S. can be non-negligible.

#### 3.4. O<sub>3</sub> transported aloft and its potential surface impact

##### 3.4.1. WRF-STILT analysis

Here we assess the possible surface impact of the high O<sub>3</sub> lamina aloft observed by AJAX on 30 May 2012 by simulating trajectories using the WRF-STILT model.

Fig. 10 gives the particle locations backward (left) and forward (right) in time as a function of altitude and time (0–48 h) release from 37.15 °N, 122.65 °W at 3 km (the same as location A in Fig. 2). The particle ensemble size is chosen as 500, but no large difference

in simulation when using larger (smaller) ensembles such as 2000 (200). The sensitivity test for this size is well documented in Mallia et al. (2014). For time-backward simulation starting at the altitude where the high O<sub>3</sub> lamina offshore was detected, all the particles come from the higher altitude (see Fig. 10 (a, c, e)). The forward time simulation, however, shows that the particles at the high O<sub>3</sub> region can transport to a broad surface region of central CA, implying the influence of upstream O<sub>3</sub> on the downstream concentration (see Fig. 10 (b, d, f)). Note that for the time-forward simulation, the potential surface influence can be significant as the particles offshore (~3 km above ground level (a.g.l.)) are transported into the downstream surface regions over CA within 1–2 days (see gray shaded region in Fig. 10b). Together with Fig. 2, time-backward simulation using STILT indicates that high O<sub>3</sub> observed at the sampled locations is not strongly associated with local North American sources, but is linked to the transport aloft, including transport from Asia. In the meanwhile, time-forward simulation using the STILT model indicates that O<sub>3</sub> transport aloft can affect the surface O<sub>3</sub> concentration in CA.

#### 3.4.2. Surface O<sub>3</sub> measurement and the upstream influence

To further investigate how high altitude O<sub>3</sub> leads to enhanced surface O<sub>3</sub> during this time, two weeks of ozone measurements

from five rural surface sites in CA are shown in Fig. 11. Three datasets (Pinnacles (PIN, 36.48 °N, 121.2 °W), Sequoia (SEK, 36.5 °N, 118.8 °W) and Yosemite (YOS, 37.85 °N, 119.55 °W) National Parks in CA) were obtained from CASTNET (<https://www.epa.gov/castnet>) and two (Merced (37.3 °N, 120.5 °W) and Visalia, 36.3 °N, 119.3 °W) were obtained from San Joaquin Valley (SJV) California Air Resources Board (CARB) (<https://www.arb.ca.gov>). Hourly measurements from Merced and Visalia were converted into the 8-hourly maximum daily average (MDA8). Fig. 11 shows O<sub>3</sub> MDA8 increased between 28 May 2012 and 1 June 2012 at all five sites. For more detailed analysis of CASTNET surface O<sub>3</sub>, see Yates et al. (2016, in review).

The time-forward particle locations shown by STILT (Fig. 10) and several surface O<sub>3</sub> measurements (Fig. 11) imply that the high O<sub>3</sub> aloft at 1.5–4 km can affect the surface O<sub>3</sub> concentration through vertical and horizontal transport. This is consistent with the findings of Yates et al. (2014), reporting that i) southern SJV O<sub>3</sub> surface sites show a shift towards maximum correlations at time-offsets that increase with distance along the valley, and ii) O<sub>3</sub> at high elevation surface sites shows significant correlation with higher offshore altitudes (2.5–4 km a.s.l.). Here we extend the modelling analysis of in-situ airborne O<sub>3</sub> data using STILT modelling to provide a helpful insight into understanding the possible causes of these

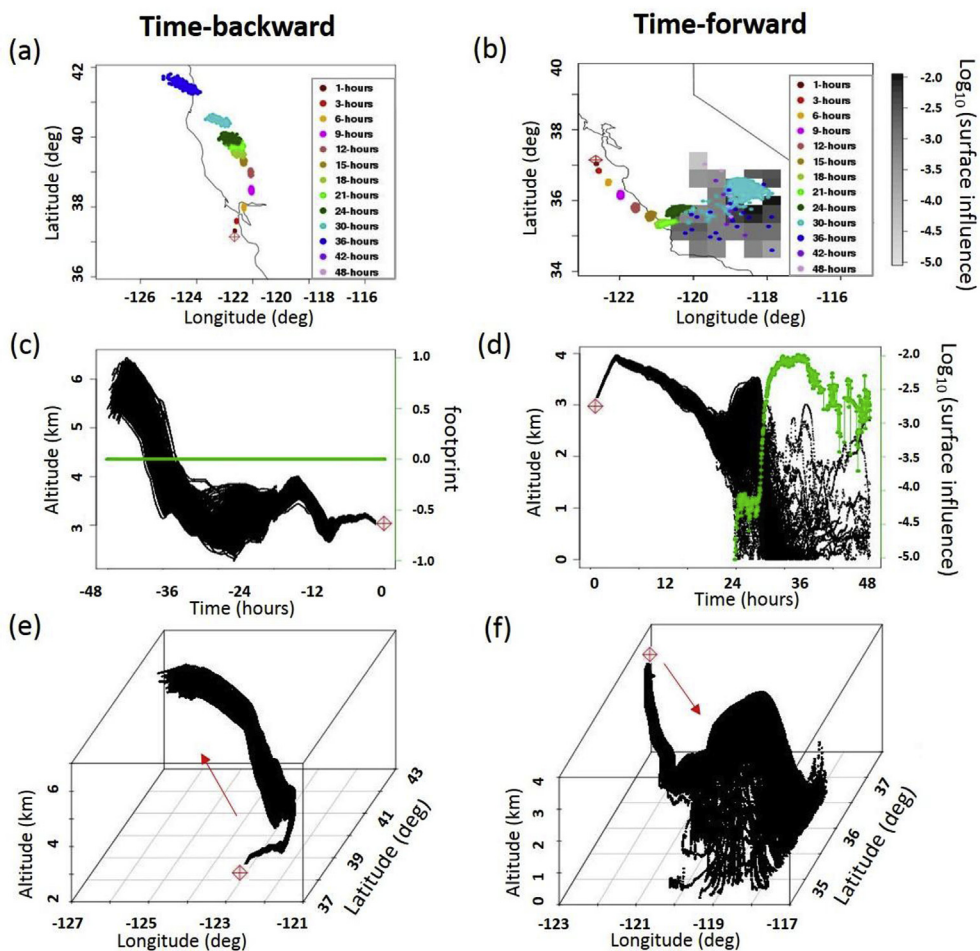


**Fig. 10.** The horizontal map of particle locations, vertical evolution of particles with time, and 3-D view of particle locations simulated (a, c, e) backward and (b, d, f) forward in time for 2 days (48 hr) starting on 30 May 2012 at 20 UTC. The particles are released at 37.15 °N, 122.65 °W, at 3 km above ground level (a.g.l.). The gray-shaded area in (b) and green dotted line in (d) shows the possible surface influence area (the sensitivity of the concentration change to the surface flux, in ppm/(μmol m<sup>-2</sup>s<sup>-1</sup>)) derived from particle locations simulated by STILT model. The gray scale is logarithm base 10 of the surface influence in each 1/4° latitude by 1/4° longitude gridcell. The darker (lighter) color represents has more (less) surface influence. The green solid line in (c) represent the footprint simulated by STILT backward in time. The red-cross diamonds represent the releasing points of the parcel at each panel. The arrow in (e, f) represents the direction of simulation starting from release point. (For interpretation of the references to colour in this figure legend, the reader is referred to the web version of this article.)

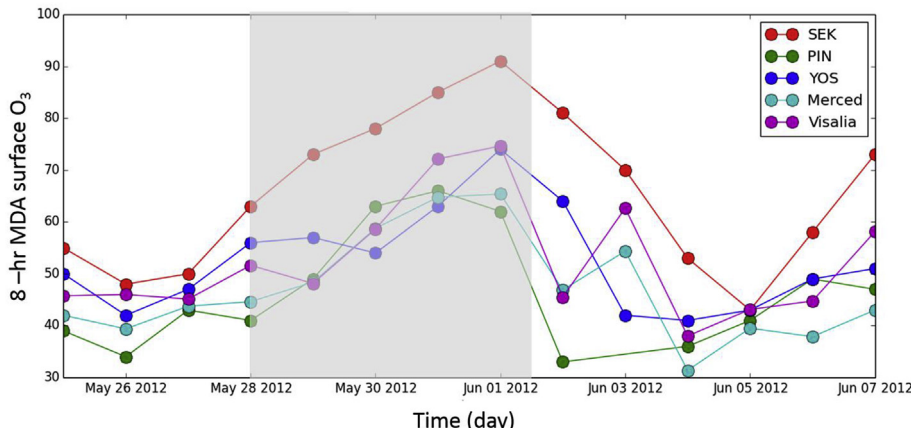


**Fig. 11.** Time series of 8-hr MDA surface O<sub>3</sub> measurements [ppb] from Sequoia (SEK), Pinnacles (PIN), and Yosemite (YOS) National Parks, and San Joaquin Valley (Merced, Visalia) sites in CA. The gray shaded area highlights the time window between 28 May 2012 and 1 June 2012.

high O<sub>3</sub> aloft, as well as predicting the potential impact on the air quality in the CA boundary layer.

#### 4. Summary and conclusions

Here we have studied a high ozone (O<sub>3</sub>) episodic event detected by the airborne Alpha Jet Atmospheric eXperiment (AJAX) on 30 May 2012, and analyzed the sources using multiple analyses including the regional-scale GEOS-Chem, MERRA-2 reanalysis data, NASA GSFC back trajectory model, and WRF-STILT model. We found that the elevated O<sub>3</sub> off the coast of the San Francisco Bay Area can be attributed primarily to a combination of downward transport from the upper troposphere and lower stratosphere through intrusions, and long-range transport of Asian pollution. GEOS-Chem simulation indicates the contributions from local/North American sources are likely small. The high MERRA-2 PV observed at low altitudes is only partially due to stratospheric intrusion, because the air inside the high PV region is moist. Thus, the 30 May 2012 stratospheric intrusion was not the sole source of O<sub>3</sub> delivered to the CA coastal region. In addition, long-range transport from Asia had an important influence on the O<sub>3</sub> pollution over the western U.S.

A back-trajectory model was used to determine the air mass origins and how much they contributed to the O<sub>3</sub> in CA. Using Q diagnostic, we quantify how and where the mixing among the air masses from different altitudes and locations occurred. The vertical motions of trajectories combined with Q diagnostic clearly demonstrate that pollution is exported from the Asian boundary layer to the free troposphere, mixed with air masses from the other altitudes, and descended to the western U.S. across the Pacific. The relative number of trajectories coming from the upper troposphere and lower stratosphere (UT/LS) is low (5%) compared to that from the lower troposphere (LT) (19%), and the relative O<sub>3</sub> mixing ratio coming from UT/LS is also still low (14%) compared to that from the LT (21%). The contribution of air parcels from the mid troposphere (MT) is dominant in terms of both the number of the trajectories (76%) and the O<sub>3</sub> mixing ratio (65%), showing that the majority (2/3) of parcels and O<sub>3</sub> near the measured sites for this case was transported aloft. The air masses coming from the LT appear to be mostly originating from Asia. MERRA-2 assimilated O<sub>3</sub> and the reconstructed O<sub>3</sub> along the trajectories underestimate measured O<sub>3</sub> by 3–12 ppbv, which shows the difficulty in capturing the fine structure of O<sub>3</sub> in the western U.S. with models.

The potential surface impact is also investigated using the WRF-STILT model and surface O<sub>3</sub> data. The particle locations and influence maps as well as the increasing surface O<sub>3</sub> leading up to the

airborne measurement day show that the observed high O<sub>3</sub>, considered to be transported aloft, affects the surface O<sub>3</sub> concentration through vertical and horizontal transport within a few days. Although the duration of the influence may vary depending on the seasons and the given synoptic conditions, it is certain that O<sub>3</sub> transported aloft has an influence on the surface O<sub>3</sub>. The actual magnitude of its effect on the surface O<sub>3</sub> remains to be a topic for a future study, though.

This case study demonstrates, through the combination of observations and multiple modeling systems, that the attribution of lower altitude O<sub>3</sub> concentrations to stratospheric origins is not always a simple assignment. Thus, systematic studies are needed to identify the magnitude of influence of Asian pollution on the western U.S. in the future. Many model and measurement studies clearly show that the transport and entrainment of trace gases from the free troposphere to the boundary layer are complex and different depending on the atmospheric conditions and geographical characteristics, but all agree in terms of the influence of Asian pollution on downstream regions. Since the distribution, the magnitude of concentration, and the transport patterns of trace gases are highly affected by the geographical distribution, season, and meteorological characteristics, it will be important to establish generalized and objective guidelines to identify the impact of Asian pollution.

Now we are facing the era in which air pollution causes not only a local problem, but also influences the whole world. Ozone over the west coast of the U.S. is influenced by the hemispheric concentrations of O<sub>3</sub> in the free troposphere through large-scale and meso-scale atmospheric processes, and can be significantly affected by emissions from Asia through long-range transport. Thus, continued studies need to collect more evidence and develop additional tools, such as the Q diagnostic, for identifying the influence of upwind emissions that may be transported in tandem with stratospheric ozone. Such data and tools would certainly provide useful information to air quality managers and policy makers.

#### Acknowledgement

The authors are grateful for the support and partnership of H211 L.L.C., and give thanks to K. Ambrose, R. Simone, B. Quiambao, J. Lee and R. Fisher. Technical contributions from Z. Young, E. Quigley, R. Walker, and A. Trias made this project possible. We give special thanks to R. Bradley Pierce (NOAA) for helping to improve the paper with insightful comments. We also thank Jovan M. Tadić, Max Loewenstein and Tomoaki Tanaka for instrumentation and data processing. Funding was provided by the NASA Postdoctoral

Program and the Bay Area Environmental Research Institute. Funding for instrumentation and aircraft integration is gratefully acknowledged from Ames Research Center Director's funds. Resources supporting this work were provided by the NASA High-End Computing (HEC) Program through the NASA Advanced Supercomputing (NAS) Division at NASA Ames Research Center. MERRA and MERRA-2 data have been provided by the GMAO at NASA's Goddard Space Flight Center through the NASA GES DISC online archive. The Global Fire Emissions Database, Version 4.0 (GFED4) data have been obtained through GFED web site (<http://www.globalfiredata.org/data.html>). The Measurements of Pollution in the Troposphere (MOPITT) version 6 product is available through the MOPITT website (<https://www2.acm.ucar.edu/mopitt>) and ASDC (Atmospheric Science Data Center) data pool. The NOAA spatially and temporally interpolated OLR were obtained from the NOAA-CIRES Climate Diagnostics Center (<http://www.cdc.noaa.gov/>). The authors thank two anonymous reviewers for their insightful comments which greatly improved this manuscript.

## Appendix A. Supplementary data

Supplementary data related to this article can be found at <http://dx.doi.org/10.1016/j.atmosenv.2017.02.008>.

## References

- Ambrose, J.L., Reidmiller, D.R., Jaffe, D.A., 2011. Causes of high O<sub>3</sub> in the lower free troposphere over the Pacific Northwest as observed at Mt. Bachelor Observatory. *Atmos. Environ.* 45, 5302–5315. <http://dx.doi.org/10.1016/j.atmosenv.2011.06.056>.
- Bey, I., Jacob, D.J., Yantosca, R.M., Logan, J.A., Field, B., Fiore, A.M., Li, Q., Liu, H., Mickley, L.J., Schultz, M., 2001. Global modeling of tropospheric chemistry with assimilated meteorology: model description and evaluation. *J. Geophys. Res.* 106, 23,073–23,096.
- Bosilovich, M.G., Robertson, F.R., Chen, J., 2011. Global energy and water budgets in MERRA. *J. Clim.* 24 (MERRA Special Issue) [10.1175/2011JCLI4175.1].
- Bosilovich, M.G., Lucchesi, R., Suarez, M., 2016. MERRA-2: File Specification. GMAO Office Note No. 9 (Version 1.1), 73 pp, available from. [http://gmao.gsfc.nasa.gov/pubs/office\\_notes](http://gmao.gsfc.nasa.gov/pubs/office_notes).
- Bourqui, M.S., Trépanier, P.-Y., 2010. Descent of deep stratospheric intrusions during the IONS August 2006 campaign. *J. Geophys. Res.* 115, D18301. <http://dx.doi.org/10.1029/2009JD013183>.
- Brown-Steiner, B., Hess, P., 2011. Asian influence on surface ozone in the United States: a comparison of chemistry, seasonality, and transport mechanisms. *J. Geophys. Res.* 116, D17309. <http://dx.doi.org/10.1029/2011JD015846>.
- Carmichael, G.R., et al., 2003. Regional-scale chemical transport modeling in support of the analysis of observations obtained during the TRACE-P experiment. *J. Geophys. Res.* 108 (D21), 8823. <http://dx.doi.org/10.1029/2002JD003117>.
- Chen, Y., Zhao, C., Zhang, Q., Deng, Z., Huang, M., Ma, X., 2009. Aircraft study of mountain chimney effect of Beijing, China. *J. Geophys. Res.* 114, D08306. <http://dx.doi.org/10.1029/2008JD010610>.
- Chung, Y.S., Dann, T., 1985. Observations of stratospheric ozone at the ground level in Regina, Canada. *Atmos. Environ.* 19, 157–162. [http://dx.doi.org/10.1016/0004-6981\(85\)90147-7](http://dx.doi.org/10.1016/0004-6981(85)90147-7).
- Cooper, O.R., et al., 2004a. A case study of transpacific warm conveyor belt transport: influence of merging airstreams on trace gas import to North America. *J. Geophys. Res.* 109, D23S08. <http://dx.doi.org/10.1029/2003JD003624>.
- Cooper, O.R., et al., 2004b. On the life cycle of a stratospheric intrusion and its dispersion into polluted warm conveyor belts. *J. Geophys. Res.* 109, D23S09. <http://dx.doi.org/10.1029/2003JD004006>.
- Cooper, O.R., Stohl, A., Hübber, G., Hsie, E.Y., Parrish, D.D., Tuck, A.F., Kiladis, G.N., Oltmans, S.J., Johnson, B.J., Shapiro, A., Moody, J.L., Lefohn, A.S., 2005. Direct transport of midlatitude stratospheric ozone into the lower troposphere and marine boundary layer of the tropical Pacific Ocean. *J. Geophys. Res.* 110, D23310. <http://dx.doi.org/10.1029/2005JD005783>.
- Cooper, O.R., et al., 2010. Increasing springtime ozone mixing ratios in the free troposphere over western North America. *Nature* 463, 344–348. <http://dx.doi.org/10.1038/nature08708>.
- Cooper, O.R., Oltmans, S.J., Johnson, B.J., Brioude, J., Angevine, W., Trainer, M., Parrish, D.D., Ryerson, T.R., Pollack, I., Cullis, P.D., Ives, M.A., Tarasick, D.W., Al-Saadi, J., Stajner, I., 2011. Measurement of western U.S. baseline ozone from the surface to the tropopause and assessment of downwind impact regions. *J. Geophys. Res.* 116, D00V03. <http://dx.doi.org/10.1029/2011JD016095>.
- Ding, A., et al., 2009. Transport of north China air pollution by midlatitude cyclones: case study of aircraft measurements in summer 2007. *J. Geophys. Res.* 114, D08304. <http://dx.doi.org/10.1029/2008JD011023>.
- Draxler, R.R., Hess, G.D., 1997. Description of the HYSPLIT\_4 Modeling System. NOAA Tech. Memo. ERL ARL-224. NOAA Air Resources Laboratory, Silver Spring, MD, 24 pp.
- Draxler, R.R., Hess, G.D., 1998. An overview of the HYSPLIT\_4 modeling system of trajectories, dispersion, and deposition. *Aust. Meteor. Mag.* 47, 295–308.
- Emery, C., Jung, J., Downey, N., Johnson, J., Jimenez, M., Yarwood, G., Morris, R., 2012. Regional and global modeling estimates of policy relevant background ozone over the United States. *Atmos. Environ.* 47, 206–217. <http://dx.doi.org/10.1016/j.atmosenv.2011.11.012>.
- Ewing, S.A., et al., 2010. Pb Isotopes as an indicator of the Asian contribution to particulate air pollution in urban California. *Environ. Sci. Technol.* 44 (23), 8911–8916. <http://dx.doi.org/10.1021/es101450t>.
- Fairlie, T.D., Avery, M.A., Pierce, R.B., Al-Saadi, J., Dibb, J., Sachse, G., 2007. Impact of multiscale dynamical processes and mixing on the chemical composition of the upper troposphere and lower stratosphere during the intercontinental chemical transport experiment—North America. *J. Geophys. Res. Atmos.* 112, D16590. <http://dx.doi.org/10.1029/2006JD007923>.
- Fine, R., et al., 2015. Investigating the influence of long-range transport on surface O<sub>3</sub> in Nevada, USA, using observations from multiple measurement platforms. *Sci. Total Environ.* <http://dx.doi.org/10.1016/j.scitotenv.2015.03.125>.
- Fiore, A.M., Jacob, D.J., Bey, I., Yantosca, R.M., Field, B.D., Fusco, A.C., Wilkinston, J.G., 2002. Background ozone over the United States in summer: origin, trend, and contribution to pollution episodes. *J. Geophys. Res.* 107 (D15), 4275. <http://dx.doi.org/10.1029/2001JD000982>.
- Fiore, A.M., Jacob, D.J., Liu, H., Yantosca, R.M., Fairlie, T.D., Li, Q., 2003. Variability in surface ozone background over the United States: implications for air quality policy. *J. Geophys. Res.* 108, 4787. <http://dx.doi.org/10.1029/2003JD003855>.
- Giglio, L., Randerson, J.T., van der Werf, G.R., 2013. Analysis of daily, monthly, and annual burned area using the fourth generation Global Fire Emissions Database (GFED4). *J. Geophys. Res. Biogeosciences.* <http://dx.doi.org/10.1002/jgrg.20042>.
- Goldstein, A.H., et al., 2004. Impact of Asian emissions on observations at Trinidad Head, California, during ITCT 2K2. *J. Geophys. Res.* 109, D23S17. <http://dx.doi.org/10.1029/2003JD004406>.
- Hamill, P., Iraci, L.T., Yates, E.L., Gore, W., Bui, T.P., Tanaka, T., Loewenstein, M., 2016. A New instrumented airborne platform for atmospheric research. *BAMS.* <http://dx.doi.org/10.1175/BAMS-D-14-00241.1>.
- Hegarty, J., Nehrkorn, T., Eluszkiewicz, J., Henderson, J., Leidner, M., Mountain, M., Draxler, R., Stein, A., Ngan, F., Brioude, J., McKain, K., Wofsy, S., DeCola, P., Jones, T., Andrews, A., 2013. Recent advances in high-resolution Lagrangian transport modeling. In: 12<sup>th</sup> Annual CMAS Conference. Chapel Hill, NC, Oct 28–30, 2013.
- Haynes, P.H., 1990. High-resolution three-dimensional modeling of stratospheric flows: quasi-two-dimensional turbulence dominated by a single vortex. In: Moffatt, H.K., Tsinober, A. (Eds.), *Topological Fluid Mechanics*. Cambridge Univ. Press, New York, pp. 345–354.
- Huang, M., et al., 2010. Impacts of transported background ozone on California air quality during the ARCTAS-CARB period a multi-scale modeling study. *Atmos. Chem. Phys.* 10, 6947–6968. <http://dx.doi.org/10.5194/acp-10-6947-2010>.
- Husar, R., et al., 2001. Asian dust events of April 1998. *J. Geophys. Res.* 106 (D16), 18,317–18,330. <http://dx.doi.org/10.1029/2000JD900788>.
- Hoskins, B.J., McIntyre, M.E., Robertson, A.W., 1985. On the use and significance of isentropic potential vorticity maps. *Q. J. R. Meteorol. Soc.* 111, 877–946.
- Jaffe, D.A., Parrish, D., Goldstein, A., Price, H., Harris, J., 2003a. Increasing background ozone during spring on the west coast of North America. *Geophys. Res. Lett.* 30 (12), 1613. <http://dx.doi.org/10.1029/2003GL017024>.
- Jaffe, D., Snow, J., Cooper, O., 2003b. The 2001 Asian dust events: transport and impact on surface aerosol concentrations in the U.S. *Eos Trans. AGU* 84 (46), 501. <http://dx.doi.org/10.1029/2003EO460001>.
- Kalnay, E., et al., 1996. The NCEP/NCAR 40-year reanalysis project. *Bull. Am. Meteorol. Soc.* 77 (3), 437–471.
- Langford, A.O., Aikin, K.C., Eubank, C.S., Williams, E.J., 2009. Stratospheric contribution to high surface ozone in Colorado during springtime. *Geophys. Res. Lett.* 36, L12801. <http://dx.doi.org/10.1029/2009GL038367>.
- Langford, A.O., Brioude, J., Cooper, O.R., Senff, C.J., Alvarez II, R.J., Hardesty, R.M., Johnson, B.J., Oltmans, S.J., 2012. Stratospheric influence on surface ozone in the Los Angeles area during late spring and early summer of 2010. *J. Geophys. Res.* 117, D00V06. <http://dx.doi.org/10.1029/2011JD016766>.
- Lamarque, J.F., Hess, P.G., 1994. Cross-tropopause mass exchange and potential vorticity budget in a simulated tropopause folding. *J. Atmos. Sci.* 51, 2246–2268.
- Lefohn, A.S., Wernli, H., Shadwick, D., Limbach, S., Oltmans, S.J., Shapiro, M., 2011. The importance of stratospheric-tropospheric transport in affecting surface ozone concentrations in the Western and Northern Tier of the United States. *Atmos. Environ.* 45, 4845–4857.
- Lefohn, A.S., Wernli, H., Shadwick, D., Oltmans, S.J., Shapiro, M., 2012. Quantifying the frequency of stratospheric-tropospheric transport affecting enhanced surface ozone concentrations at high- and low-elevation monitoring sites in the United States. *Atmos. Environ.* 62, 646–656.
- Lefohn, A., Emery, C., Shadwick, D., Wernli, H., Jung, J., Oltmans, S.J., 2014. Estimates of background surface ozone concentrations in the United States based on model-derived source apportionment. *Atmos. Environ.* 84, 275–288.
- Levett, P.F., Oord, G.H.J.V.D., Dobber, M.R., Mälki, A., Visser, H., Vries, J.D., Stammes, P., Lundell, J.O.V., Saari, H., 2006. The ozone monitoring instrument. *IEEE Trans. Geosci. Remote Sens.* 44, 1093–1101. <http://dx.doi.org/10.1109/TGRS.2006.872333>.
- Liebmann, B., Smith, C.A., 1996. Description of a complete (interpolated) outgoing longwave radiation dataset. *Bull. Am. Meteorological Soc.* 77, 1275–1277.

- Lin, J.-T., McElroy, M.B., 2010. Impacts of boundary layer mixing on pollutant vertical profiles in the lower troposphere: implications to satellite remote sensing. *Atmos. Environ.* 44, 1726–1739.
- Lin, S.-J., Rood, R.B., 1996. Multidimensional flux-form semi-lagrangian transport schemes. *Mon. Wea. Rev.* 124, p2046–2070.
- Lin, M., Holloway, T., Carmichael, G.R., Fiore, A.M., 2010. Quantifying pollution inflow and outflow over East Asia in spring with regional and global models. *Atmos. Chem. Phys.* 10, 4221–4239. <http://dx.doi.org/10.5194/acp-10-4221-2010>.
- Lin, M., Fiore, A.M., Horowitz, L.W., Cooper, O.R., Naik, V., Holloway, J., Johnson, B.J., Middlebrook, A.M., Oltmans, S.J., Pollack, I.B., Ryerson, T.B., Warner, J.X., Wiedinmyer, C., Wilson, J., Wyman, B., 2012a. Transport of Asian ozone pollution into surface air over the western United States in spring. *J. Geophys. Res.* 117, D00V07. <http://dx.doi.org/10.1029/2011JD016961>.
- Lin, M., Fiore, A.M., Cooper, O.R., Horowitz, L.W., Langford, A.O., Levy II, H., Johnson, B.J., Naik, V., Oltmans, S.J., Senff, C.J., 2012b. Springtime high surface ozone events over the western United States: quantifying the role of stratospheric intrusions. *J. Geophys. Res.* 117, D00V22. <http://dx.doi.org/10.1029/2012JD018151>.
- Lin, M., Horowitz, L.W., Cooper, O.R., Tarasick, D., Conley, S., Iraci, L.T., Johnson, B., Leblanc, T., Petropavlovskikh, I., Yates, E.L., 2015. Revisiting the evidence of increasing springtime ozone mixing ratios in the free troposphere over western North America. *Geophys. Res. Lett.* 42, 8719–8728. <http://dx.doi.org/10.1002/2015GL065311>.
- Lin, J.C., Gerbig, C., Wofsy, S.C., Andrews, A.E., Daube, B.C., Davis, K.J., Grainger, C.A., 2003. A near-field tool for simulating the upstream influence of atmospheric observations. *J. Geophys. Res.* 108 (A12), 1–17. <http://dx.doi.org/10.1029/2002JD003161>.
- Liu, H.Y., et al., 2003. Transport pathways for Asian pollution outflow over the Pacific: interannual and seasonal variations. *J. Geophys. Res.* 108 (D20), 8786. <http://dx.doi.org/10.1029/2002JD003102>.
- Mallia, D.V., Lin, J.C., Urbanski, S., Ehleringer, J., Nehrkorn, T., 2014. Impacts of upwind wildfire emissions on CO, CO<sub>2</sub>, and PM2.5 concentrations in Salt Lake City, Utah. *J. Geophys. R.* 120, 147–166 doi:10.1002/2014JD022472.
- McKendry, G., et al., 2008. Trans-pacific dust events observed at whistler, british columbia during INTEX-B. *Atmos. Chem. Phys.* 8, 6297–6307. <http://dx.doi.org/10.5194/acp-8-6297-2008>.
- Mesinger, F., Dimego, G., Kalnay, E., Kenneth, M., Shafran, P.C., Ebjsuzaki, W., Jovic, D., Woollen, J., Rogers, E., Berbery, E.H., Ek, M.B., Fan, Y., Grumbine, R., Higgins, W., Li, H., Lin, Y., Mankin, G., Parrish, D., Shi, W., 2006. North American regional reanalysis. *BAMS* 343–360.
- Moncrieff, M.W., Shapiro, M.A., Slingo, J.M., Molteni, F., 2007. Collaborative research at the intersection of weather and climate. *World Meteorol. Organ. Bull.* 56 (3), 204–211.
- Nehrkorn, T., Eluszkiewicz, J., Wofsy, S.C., Lin, J.C., Gerbig, C., Longo, M., Freitas, S., 2010. Coupled weather research and forecasting–stochastic time-inverted lagrangian transport (WRF–STILT) model. *Meteorol. Atmos. Phys.* 2010 (107), 51–64. <http://dx.doi.org/10.1007/s00703-010-0068-x>.
- Ohara, T., Akimoto, H., Kurokawa, J., Horii, N., Yamaji, K., Yan, X., Hayasaka, T., 2007. An Asian emission inventory of anthropogenic emission sources for the period 1980–2020. *Atmos. Chem. Phys.* 7, 4419–4444. <http://dx.doi.org/10.5194/acp-7-4419-2007>.
- Oltmans, S.J., Lefohn, A.S., Harris, J.M., Shadwick, D.S., 2008. Background ozone levels of air entering the west coast of the U.S. and assessment of longer-term changes. *Atmos. Environ.* 42, 6020–6038. <http://dx.doi.org/10.1016/j.atmosenv.2008.03.034>.
- Ott, L.E., et al., 2016. Frequency and impact of summertime stratospheric intrusions over Maryland during DISCOVER-AQ (2011): new evidence from NASA's GEOS-5 simulations. *J. Geophys. Res. Atmos.* 121, 3687–3706. <http://dx.doi.org/10.1002/2015JD024052>.
- Parrish, D.D., Millet, D.B., Goldstein, A.H., 2009. Increasing ozone in marine boundary layer inflow at the west coasts of North America and Europe. *Atmos. Chem. Phys.* 9, 1303–1323. <http://dx.doi.org/10.5194/acp-9-1303-2009>.
- Parrish, D.D., Aikin, K.C., Oltmans, S.J., Johnson, B.J., Ives, M., Sweeny, C., 2010. Impact of transported background ozone inflow on summertime air quality in a California ozone exceedance area. *Atmos. Chem. Phys.* 10, 10,093–10,109. <http://dx.doi.org/10.5194/acp-10-10093-2010>.
- Pfister, G.G., et al., 2011. Characterizing summertime chemical boundary conditions for airmasses entering the US West coast. *Atmos. Chem. Phys.* 11, 1769–1790. <http://dx.doi.org/10.5194/acp-11-1769-2011>.
- Rastigjev, Y., Park, R., Brenner, M.P., Jacob, D.J., 2010. Resolving intercontinental pollution plumes in global models of atmospheric transport. *J. Geophys. Res.* 115, D02302. <http://dx.doi.org/10.1029/2009JD012568>.
- Richter, A., et al., 2005. Increase in tropospheric nitrogen dioxide over China observed from space. *Nature* 437 (7055), 129–132. <http://dx.doi.org/10.1038/nature04092>.
- Roca, R., Lafore, J.-P., Piriou, C., Redelsperger, J.L., 2005. Extratropical dry-air intrusions into the West African Monsoon Midtroposphere: an important factor for the convective activity over the Sahel. *J. Atmos.* 62, 390–407.
- Ryall, D.B., Derwent, R.G., Manning, A.J., Simmonds, P.G., O'Doherty, S., 2001. Estimating source regions of European emissions of trace gases from observations at mace head. *Atmos. Environ.* 35, 1507–1512, 2001.
- Ryoo, J.-M., Waugh, D.W., Gettelman, A., 2008. Variability of subtropical upper tropospheric humidity. *Atmos. Chem. Phys.* 8, 2643–2655.
- Ryoo, J.-M., Waliser, D.E., Waugh, D.W., Wong, S., Fetzer, E.J., Fung, I., 2015. Classification of atmospheric river events on the U.S. West Coast using a trajectory model. *J. Geophys. Res. Atmos.* 120 <http://dx.doi.org/10.1002/2014JD022023>.
- Schoeberl, M.R., Sparling, L., 1995. Trajectory modeling, in diagnostic tools in atmospheric physics. In: Fiocco, G., Visconti, G. (Eds.), *Proc. Int. Sch. Phys. "Enrico Fermi*, vol. 124, pp. 289–306.
- Shapiro, M.A., 1980. Turbulent mixing within tropopause folds as a mechanism for the exchange of chemical constituents between the stratosphere and the troposphere. *J. Atmos. Sci.* 37, 994–1004.
- Simmons, A., Uppala, S., Dee, D., Kobayashi, S., 2007. ERA-Interim: new ECMWF reanalysis products from 1989 onwards. *ECMWF Newsl.* 110, 1–53.
- Skamarock, W.C., Klemp, J.B., 2008. A time-split nonhydrostatic atmospheric model for weather research and forecasting applications. *J. Comput. Phys.* 227, 3465–3485.
- Skamarock, W.C., Klemp, J.B., Dudhia, J., Gill, D.O., Barker, D.M., Duda, M.G., Huang, X.-Y., Wang, W., Powers, J.G., 2008. A Description of the Advanced Research WRF Version 3 (NCAR Technical note, June).
- Stohl, A., 1998. Computation, accuracy and applications of trajectories—a review and bibliography. *Atmos. Environ.* 32, 947–966.
- Suarez, M., Bacmeister, J., 2015. Development of the GEOS-5 atmospheric general circulation model: evolution from MERRA to MERRA2. *Geosci. Model Dev.* 8, 1339–1356. <http://dx.doi.org/10.5194/gmd-8-1339-2015>.
- US Environmental Protection Agency US EPA, 2015. National ambient air quality standards for ozone. *Fed. Regist.* 80 (No. 206). <https://www.gpo.gov/fdsys/pkg/FR-2015-10-26/pdf/2015-26594.pdf>.
- van der Werf, G.R., Randerson, J.T., Giglio, L., Collatz, G.J., Mu, M., Kasibhatla, P.S., Morton, D.C., DeFries, R.S., Jin, Y., van Leeuwen, T.T., 2010. Global fire emissions and the contribution of deforestation, savanna, forest, agricultural, and peat fires (1997–2009). *Atmos. Chem. Phys.* 10, 11707–11735. <http://dx.doi.org/10.5194/acp-10-11707-2010>.
- Verstraeten, W.W., New, J.L., Williams, J.E., Bowman, K.W., Worden, J.R., Boersma, K.F., 2015. Rapid increases in tropospheric ozone production and export from China. *Nat. Geosci.* <http://dx.doi.org/10.1038/NGEO2493>.
- Waters, J.W., et al., 2006. The Earth observing system microwave limb sounder (EOS MLS) on the Aura satellite. *IEEE Trans. Geosci. Remote Sens.* 44, 1075–1092.
- Weiss-Penzias, P., et al., 2007. Quantifying Asian and biomass burning sources of mercury using the Hg/CO ratio in pollution plumes observed at the Mount Bachelor observatory. *Atmos. Environ.* 41 (21), 4366–4379. <http://dx.doi.org/10.1016/j.atmosenv.2007.01.058>.
- Wargan, K., Pawson, S., Olsen, M.A., Witte, J.C., Douglass, A.R., Ziemke, J.R., Strahan, S.E., Nielsen, J.E., 2015. The global structure of upper troposphere–lower stratosphere ozone in GEOS-5: a multiyear assimilation of EOS Aura data. *J. Geophys. Res. Atmos.* 120, 2013–2036. <http://dx.doi.org/10.1002/2014JD022493>.
- Waugh, D.W., 2005. Impact of potential vorticity intrusions on subtropical upper tropospheric humidity. *J. Geophys. Res.* 110, D11305. <http://dx.doi.org/10.1029/2004JD005664>.
- Wright, J.S., Fu, R., Fueglistaler, S., Liu, Y.S., Zhang, Y., 2011. The influence of summertime convection over Southeast Asia on water vapor in the tropical stratosphere. *J. Geophys. Res.* 116, D12302. <http://dx.doi.org/10.1029/2010JD015416>.
- Yates, E.L., Iraci, L.T., Roby, M.C., Pierce, R.B., Johnson, M.S., Reddy, R.J., Tadic, J.M., Loewenstein, M., Gore, W., 2013. Airborne observations and modeling of springtime stratosphere-to-troposphere transport over California. *Atmos. Chem. Phys.* 13, 12481–12494. <http://dx.doi.org/10.5194/acp-13-12481-2013>.
- Yates, E.L., Iraci, L.T., Austerberry, D., Pierce, R.B., Roby, M.C., Tadic, J.M., Loewenstein, M., Gore, W., 2014. Characterizing the impacts of vertical transport and photochemical ozone production on an exceedance area. *Atmos. Environ.* <http://dx.doi.org/10.1016/j.atmosenv.2014.09.002>.
- Yates, E.L., Johnson, M.S., Iraci, L.T., Ryoo, J.-M., Pierce, R.B., Cullis, P.D., Gore, W., Ives, M.A., Johnson, B.J., Leblanc, T., Marrero, J.E., Sterling, C.W., Tanaka, T., 2016. An assessment of ground-level and free-tropospheric ozone over California and Nevada (In review). *J. Geophys. Res.*
- Yienger, J.J., Galanter, M., Holloway, T.A., Phadnis, M.J., Guttikunda, S.K., Carmichael, G.R., Moxim, W.J., Levy II, H., 2000. The episodic nature of air pollution transport from Asia to North America. *J. Geophys. Res.* 105 (D22), 26,931–26,945. <http://dx.doi.org/10.1029/2000JD900309>.
- Zhang, L., et al., 2008. Transpacific transport of ozone pollution and the effect of recent Asian emission increases on air quality in North America: an integrated analysis using satellite, aircraft, ozonesonde, and surface observations. *Atmos. Chem. Phys.* 8, 6117–6136. <http://dx.doi.org/10.5194/acp-8-6117-2008>.
- Zhang, L., Jacob, D.J., Kopacz, M., Henze, D.K., Singh, K., Jaffe, D.A., 2009. Intercontinental source attribution of ozone pollution at western U.S. sites using an adjoint method. *Geophys. Res. Lett.* 36, L11810. <http://dx.doi.org/10.1029/2009GL037950>.
- Zhang, L., Jacob, D.J., Downey, N.V., Wood, D.A., Blewitt, D., Carouge, C.C., van Donkelaar, A., Jones, D.B.A., Murray, L.T., Wang, Y., 2011. Improved estimate of the policy-relevant background ozone in the United States using the GEOS-Chem global model with 1/2°–2/3° horizontal resolution over North America. *Atmos. Environ.* 45, 6769–6776.
- Zhang, L., Jacob, D.J., Downey, N.V., Wood, D.A., Blewitt, D., 2014. Sources contributing to background surface ozone in the US Intermountain West. *Atmos. Chem. Phys.* 14, 5295–5309. <http://dx.doi.org/10.5194/acp-14-5295-2014>.
- Zhang, Q., et al., 2009. Asian emissions in 2006 for the NASA INTEX-B mission. *Atmos. Chem. Phys.* 9, 5131–5153. <http://dx.doi.org/10.5194/acp-9-5131-2009>.